

Cooling neutrons using non-dispersive magnetic excitations

O. Zimmer

Institut Laue Langevin, 38042 Grenoble, France

June 17, 2014

Abstract

A new method is proposed for cooling neutrons by inelastic magnetic scattering in weakly absorbing, cold paramagnetic systems. Kinetic neutron energy is removed in constant decrements determined by the Zeeman energy of paramagnetic atoms or ions in an external magnetic field, or by zero-field level splittings in magnetic molecules. Analytical solutions of the stationary neutron transport equation are given using inelastic neutron scattering cross sections derived in an appendix. They neglect any inelastic process except the paramagnetic scattering and hence still underestimate very-cold neutron densities. Molecular oxygen with its triplet ground state appears particularly promising, notably as a host in fully deuterated O_2 -clathrate hydrate, or more exotically, in dry O_2 - ^4He van der Waals clusters. At a neutron temperature about 6 K, for which neutron conversion to ultra-cold neutrons by single-phonon emission in pure superfluid ^4He works best, conversion rates due to paramagnetic scattering in the clathrate are found to be a factor 9 larger. While in conversion the neutron imparts only a single energy quantum to the medium, the multi-step paramagnetic cooling cascade leads to further strong enhancements of very-cold neutron densities, e.g., by a factor 14 (57) for an initial neutron temperature of 30 K (100 K), for the moderator held at about 1.3 K. Due to a favorable Bragg cutoff of the O_2 -clathrate the cascade-cooling can take effect in a moderator with linear extensions smaller than a meter. The paramagnetic cooling mechanism may offer benefits in novel intense sources of very cold neutrons and for enhancing production of ultra-cold neutrons.

Keywords: neutron scattering, neutron moderation, very cold neutrons, ultra-cold neutrons

1 Introduction

Thermal and cold neutrons play an important role for fundamental research, on one hand as a probe to study condensed matter systems and for inducing nuclear reactions, on the other hand as an object and a tool for studying low-energy particle physics via precise measurements of the static and decay properties of the neutron. Cold neutrons are commonly produced by slowdown from thermal energies, using a cold medium with a suitable dynamical structure factor and weak absorption. Liquid hydrogen and deuterium held at the respective boiling points at about 20 and 24 K are particularly effective for moderation and have gained practical importance as "cold neutron sources" implemented in high-flux neutron research facilities. For instance, a liquid-deuterium cold source at the Institut Laue Langevin (ILL) in Grenoble, France, provides a gain factor 80 – 100 for low-energy neutrons with wavelengths $\lambda > 1$ nm [1]. For further cooling of neutrons one would need a colder medium with suitable degrees of freedom. Collective excitations such as phonons in a cold solid with Debye temperature T_D are however rather inappropriate for moderation since for neutron energy, $E < k_B T_D$, the cross section for single phonon emission is proportional to $(E/k_B T_D)^3$, and cross sections for higher order processes

drop even faster with decreasing energy [2]. Localized, dispersion-free excitations on the other hand do not suffer from this limitation and may work even at lowest neutron energies.

A peculiar, forty years old proposal of "phononless cooling of neutrons to extremely low temperatures" involves tiny energy transfers in units of neutron and nuclear Zeeman energy [3]. In a moderator comprised of deuterons with nuclear spins highly polarized along a strong magnetic field, conservation of angular momentum allows simultaneous neutron and nuclear spin flips to happen only in the doublet state and hence, due to the associated positive change of Zeeman energies, only with the removal of neutron kinetic energy. Since even in magnetic fields of several Tesla this amounts to less than a μeV , many spin flip collisions will be necessary for significant neutron cooling. The author of the proposal pointed out that, even for an ideally polarized deuteron system in a field as strong as 30 T, cooling to extremely low temperatures would take effect only after preliminary cooling of the neutron spectrum to at least 12 K. These conditions explain why the proposal has not yet been put into practice. A similar situation appears in refrigeration of bulk matter to lowest temperatures using adiabatic nuclear demagnetization. A popular method to achieve the necessary precooling is adiabatic demagnetization of paramagnetic salts, which due to the large electronic magnetic moments is much better adapted for cooling at a higher temperature than a nuclear stage.

Guided by this analogy we are led to consider slowdown of neutrons due to scattering by a paramagnetic system at low temperature, which has not yet been reported in the literature. Here, the transfer of energy in a scattering process with electron spin flip is typically three orders of magnitude larger than for nuclear spin flip scattering, due to the ratio of the Bohr and nuclear magnetons. For simple paramagnetic atomic or ionic species it is determined by an external field, whereas magnetic molecules possess zero-field splittings of magnetic energy levels able to remove neutron kinetic energy even without an external field. As a consequence of the non-dispersivity of paramagnetic excitations, neutron cooling can proceed in inelastic, incoherent scattering cascades with energy decrement E^* of typically a fraction of a meV.

A particular motivation for this study is the quest for efficient production methods of neutrons in the low-energy range of the spectrum provided by a cold source, commonly called very cold neutrons (VCN) and ultra-cold neutrons (UCN). More intense beams of VCN would enhance capabilities of neutron scattering techniques such as reflectometry, spin echo spectroscopy and interferometry, to mention only some classical applications. They may also offer new opportunities for fundamental physics projects, such as beam-based searches for a non-vanishing neutron electric dipole moment (EDM) [4], for neutron-antineutron oscillations [5], or for new fundamental forces [6]. UCN on the other hand can be trapped in bottles made of materials with positive neutron optical potential, by magnetic field gradients, and by gravity [7, 8]. Owing to this peculiar property they have become a valuable tool for a plethora of investigations in fundamental physics [9, 10, 11].

A classical method for production of UCN and VCN at the ILL extracts low-energy neutrons from a liquid-deuterium moderator through a vertical neutron guide, followed by a phase space transformation to lowest energies using a neutron turbine [12]. More recently, alternative methods have begun to provide competitive UCN densities [13, 14, 15, 16, 17, 18, 19]. They involve conversion of cold neutrons in single inelastic scattering events [20], instead of multiple energy transfers characteristic for neutron slowdown in a moderator. In its simplest form the converter acts as an effective two-level system with an excited state separated by an energy E^* from the ground state. At temperatures $k_{\text{B}}T \ll E^*$ the excited state is strongly depleted, leading to a suppression of neutron up-scattering back to higher energy. Converter materials investigated so far are superfluid helium [21], solid deuterium [21, 22], solid α -oxygen [23, 24] and solid ^{15}N [25]. All cases employ phonons (with a contribution of magnons for α -oxygen), with E^* in the order of one to several meV (e.g., 1 meV for superfluid ^4He).

For paramagnetic scattering typical single energy transfers are smaller (e.g., 0.4 meV for

| Species | S | $g_-(T \rightarrow 0)$ | σ_a (mbarn) |
|----------------------|-----|------------------------|---------------------|
| electron | 1/2 | 1/3 | 0 |
| ^2H | 1/2 | 1/3 | 0.519 (7) |
| ^1H | 1/2 | 1/3 | 332.6 (7) |
| ^{15}N | 3/2 | 1 | 0.024 (8) |
| ^{14}N | 3/2 | 1 | 1910 (30) |
| $^{16}\text{O}_2$ | 1 | 4/3 | 2×0.10 (2) |
| natural O_2 | 1 | 4/3 | 2×0.19 (2) |

Table 1: Weakly absorbing paramagnetic species with electronic spin S . For atomic hydrogen and nitrogen also the strongly absorbing isotopic contaminants are quoted. The cross section for magnetic down-scattering is proportional to the thermal factor $g_-(T)$ (see eq. 1 and the appendix). Neutron absorption cross sections are quoted for neutrons with a speed of 2200 m/s.

molecular oxygen encaged in the inclusion compounds discussed below). More importantly and contrary to dispersive, collective excitations, energy transfers can be cascaded over a comb of many equidistant neutron energy groups within a broad incident neutron spectrum. Here we show that this paramagnetic cooling cascade provides an efficient channel for low-energy neutron moderation prior to a final conversion process to UCN or VCN, leading to a large enhancement of conversion rates. Particularly promising are materials involving molecular oxygen. Besides other advantages they can be kept close to the magnetic ground state at ordinary liquid-helium temperatures, which is a helpful feature for technical implementations.

2 Neutron conversion by a paramagnetic electron spin system

We start with a discussion of a paramagnetic electron spin system as a neutron converter, i.e. neglecting multiple inelastic scattering events. This situation prevails if only a small amount of material is exposed to a neutron field. Key criteria are a large density of unpaired electrons and weak neutron absorption. Paramagnetic atomic and molecular species worthwhile to be considered are listed in Table 1. They involve the nuclides ^2H , ^{16}O and ^{15}N that possess absorption cross sections $\sigma_a < 10^{-27} \text{ cm}^2$ for thermal neutrons and can be prepared in systems with paramagnetic spin densities exceeding 10^{20} cm^{-3} . Pure ^4He is the only existing medium with no absorption at all. It possesses paramagnetic states in form of single-electron bubbles and the $\text{He}_2^*(a^3\Sigma_u^+)$ excimer triplet state. Sufficient bulk density is however an obvious issue for charged or unstable species. On the other hand, the vanishing absorption makes ^4He an interesting matrix for hosting paramagnetic atoms and molecules.

For calculation of conversion rates we need cross sections for neutron scattering with an electron spin flip without neglecting the change of neutron kinetic energy due to Zeeman or molecular zero-field splittings. As they seem not to appear in the literature¹ we derive them in the appendix. We write the macroscopic, energy-differential cross section of a paramagnetic system for neutron scattering from an initial energy E (wavenumber k) to a final energy E' (wavenumber k') as

$$\Sigma^\pm(E \rightarrow E') = n_{\text{pc}} \sigma_m \frac{k'}{k} g_\pm(T) f_\pm(E) \delta(E \pm E^* - E'), \quad (1)$$

where the upper (lower) sign stands for a process with neutron energy gain (loss), n_{pc} is the

¹Magnetic neutron scattering theory serves for analyzing experimental data for investigating structure and dynamics of condensed matter systems. In paramagnetic systems the scattering associated with an electron spin flip is diffuse and thus of rather limited interest. Even in presence of magnetic fields it is usually treated as elastic, neglecting small changes of neutron kinetic energy due to Zeeman splittings [26, 27].

number density of paramagnetic centers of a single species with spin S , and $\sigma_m = 4\pi b_m^2 \approx 3.66$ barn with the magnetic scattering length as defined in eq. 55 in the appendix. For the dispersion-free excitations considered here the (positive) transfer energy E^* is independent on the neutron energy and balances a corresponding loss or gain in neutron kinetic energy. Obviously, neutron down-scattering is only possible for $E > E^*$. For paramagnetic atoms or ions with g-factor g and without crystal field splittings,

$$E^* = |g\mu_B B_0| = \frac{|g|}{2} 115.8 \mu\text{eV} \times B_0 [\text{T}] \quad (2)$$

is the Zeeman splitting of magnetic states in an external magnetic field B_0 . For the species quoted in Table 1, $g \approx -2$. With respect to the electronic Zeeman energy the neutron Zeeman energy is negligible and not taken into account here. Molecular oxygen has a paramagnetic spin triplet ground state ($^3\Sigma_g^-$). Without external magnetic field,

$$E^* = D, \quad (3)$$

where D is the zero-field splitting constant of the spin $S = 1$ states with projection $m = 0$ and $m = \pm 1$ along the molecular axis. Using electron spin resonance spectroscopy $D = 491 \mu\text{eV}$ was measured for oxygen in the gas phase [28]. Electrostatic effects on O_2 molecules embedded in a bulk matter matrix may modify this value, as noticeable in the systems discussed below. The functions $g_{\pm}(T)$ contain thermal averages of spin matrix elements and are given in the appendix. In the low temperature limit, $k_B T \ll E^*$, where the system is close to its magnetic ground state,

$$g_+(T \rightarrow 0) \rightarrow 0 \quad (4)$$

leads to suppression of neutron up-scattering, while cross sections for down-scattering become proportional to

$$g_-(T \rightarrow 0) \rightarrow \begin{cases} 2S/3 & (\text{Zeeman system}) \\ 4/3 & (\text{O}_2 \text{ molecule}) \end{cases}. \quad (5)$$

The functions $f_{\pm}(E)$ in eq. 1 account for the effect of the magnetic form factor $F(\boldsymbol{\kappa})$, which depends on the transfer wave vector $\boldsymbol{\kappa} = \mathbf{k} - \mathbf{k}'$. A theoretical expression of the magnetic form factor of gaseous oxygen based on Meckler's electron wave functions [29] was given by Kleiner [30] and found to be very similar to the form factor measured in condensed phases [31, 32]. For encaged, unoriented O_2 molecules we may write, following a discussion in ref. [30],

$$f_{\pm}(E) = \frac{1}{2} \int_0^\pi \langle |F|^2 \rangle (\kappa_{\pm}(E, \theta)) \sin \theta d\theta, \quad (6)$$

where the brackets stand for orientational averaging of the molecules. For our purposes we approximate $\langle |F|^2 \rangle$ by a Gaussian with a half width of 15 nm^{-1} at half maximum. The functional dependence of κ_{\pm} on the initial neutron energy E and the scattering angle θ is given by

$$\frac{\hbar^2}{2m_n} \kappa_{\pm}^2 = 2E \pm E^* - 2\sqrt{E(E \pm E^*)} \cos \theta. \quad (7)$$

Figure 1 shows $f_-(E)$. Note that $f_+(E) = f_-(E + E^*)$. Equation 1 should also contain the Debye-Waller factor, which for a harmonically bound center with mass M and oscillation frequency ω_0 can be written as (see, e.g., ref. [2])

$$\exp(-2W) = \exp\left(-\frac{\hbar \kappa^2}{2M\omega_0}\right). \quad (8)$$

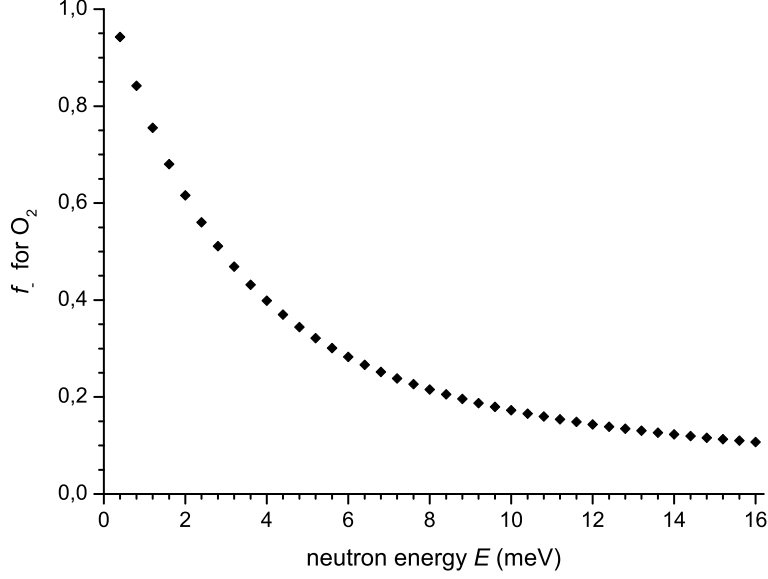


Figure 1: The function $f_-(E)$ as defined in eq. 6, describing the effect of the magnetic form factor of molecular oxygen on the neutron scattering cross section.

However, for $M \gg m_n$ and a cold system where the oscillators are in the ground state, it reduces scattering cross sections by less than a few per cent and is therefore neglected in the further analysis.

The spectral conversion rate density, i.e. the number of neutrons converted in a neutron field to energy $E' < E$, per units of time, volume and energy, is given by

$$p(E') = \int_0^\infty \Phi(E) \Sigma^-(E \rightarrow E') dE, \quad (9)$$

where $\Phi(E) dE$ denotes a spatially homogeneous incident flux of neutrons with energies in an interval of width dE about E [33]. Using eq. 1 and the relation

$$\Phi(E) = n(E) v(E), \quad (10)$$

with the spectral neutron density $n(E)$ and the neutron speed $v(E) = \sqrt{2E/m_n}$ (m_n is the neutron mass), one obtains

$$p(E') = n(E' + E^*) n_{pc} \sigma_{mg-}(T) f_-(E' + E^*) v(E'). \quad (11)$$

For the special case of conversion to UCN, we note that their energy range, $0 < E' \leq E_c$, is defined by a cutoff E_c , normally with a value less than 350 neV, e.g. due to the neutron optical potential of the wall material of a UCN bottle. Comparison with eq. 3, or with eq. 2 for not too small magnetic field, shows that $E^* \gg E_c$. The total rate density of neutron conversion to UCN follows simply from integration of eq. 11 over all UCN energies, i.e.

$$p = \int_0^{E_c} p(E') dE' = \frac{2}{3} \sqrt{\frac{2}{m_n}} n(E^*) n_{pc} \sigma_{mg-}(T) f_-(E^*) E_c^{3/2}. \quad (12)$$

Once converted, neutrons may get lost through the inverse process of up-scattering with cross section $\propto g_+(T)$ that depends on the deviation of the system from the magnetic ground

state. The corresponding spectral rate density is given by

$$\tilde{p}(E) = \int_0^\infty \Phi(E) \Sigma^+(E \rightarrow E') dE' = n(E) n_{\text{pc}} \sigma_{\text{mg}+}(T) f_+(E) v(E + E^*). \quad (13)$$

For the special case of UCN up-scattering, one obtains

$$\tilde{p} = \int_0^{E_c} \tilde{p}(E) dE = n_{\text{UCN}} n_{\text{pc}} \sigma_{\text{mg}+}(T) f_+(0) v(E^*), \quad (14)$$

where

$$n_{\text{UCN}} = \int_0^{E_c} n(E) dE \quad (15)$$

is the UCN density. Notice that in the eqs. 11 and 13 the quantity multiplied with the spectral neutron density can be interpreted as a corresponding rate constant. For conversion to neutrons with energy $E' \ll E^*$ we write it as

$$\tau_{\text{conv}}^{-1} = n_{\text{pc}} \sigma_{\text{mg}-}(T) f_-(E^*) v(E'), \quad (16)$$

and the up-scattering rate constant as

$$\tau_{\text{up}}^{-1} = n_{\text{pc}} \sigma_{\text{mg}+}(T) f_+(0) v(E^*). \quad (17)$$

Relevant is also the rate constant for neutron absorption, which is given by

$$\tau_{\text{a}}^{-1} = v \Sigma_{\text{a}}, \quad (18)$$

where Σ_{a} is the macroscopic neutron absorption cross section. In contrast to τ_{conv}^{-1} and τ_{up}^{-1} , τ_{a}^{-1} does not depend on the neutron speed, since $\Sigma_{\text{a}} \propto 1/v$.

Turning now toward a discussion of realistic paramagnetic media, we start with a material with a particularly low absorption, composed of the paramagnetic atoms or molecules listed in Table 1, implanted in a matrix of ^4He . A viable method employs injection of an impurity loaded helium gas jet into superfluid helium, which makes a jelly-like helium-impurity condensate [34]. A high frequency discharge prior to injection can lead to samples wherein impurity atoms are present with a degree of dissociation up to 50%, and still 20% for samples with highest atomic density [35]. After injection, polarizable heavy impurities can be packed in dry van der Waals clusters where the impurity is surrounded by a crust of some dozen helium atoms. For molecular nitrogen, impurity number densities up to $1.46 \times 10^{21} \text{ cm}^{-3}$ were demonstrated [36], and one can expect oxygen to behave similarly. An obvious obstacle in using the particularly weakly absorbing ^{15}N is the need for highly enriched material to suppress the large absorption of ^{14}N . This makes atomic ^{15}N but also paramagnetic nitric molecules such as ^{15}NO ($S = 1/2$) rather impractical. Isotopically pure deuterium is commercially available in large quantities but it remains to be shown experimentally that dry van der Waals clusters can be produced with sufficient abundance of ^2H atoms. However, from a look in Table 1 and also from a practical point of view there seems to be no advantage compared to molecular oxygen with natural isotopic composition.

In fact, molecular oxygen appears to be the most promising paramagnetic species. No dissociation of molecules and subsequent stabilization of atoms in the helium is needed here and, contrary to atomic Zeeman states, no magnetic field needs to be applied for lifting degeneracies of magnetic levels. The goal is to keep the O_2 molecules paramagnetic in a highly packed state, avoiding magnetic order as it appears for instance in the antiferromagnetic crystalline α phase of pure oxygen. For the maximum density achieved in the aforementioned van der Waals solid the molecules are already more than sufficiently separated. Indeed, neglecting superexchange

| Host | Cage structure | $n_{\text{pc}} \text{ (cm}^{-3}\text{)}$ | $\tau_{\text{a}}^{-1} \text{ (s}^{-1}\text{)}$ | $\tau_{\text{UCN}}^{-1} \text{ (s}^{-1}\text{)}$ | $T_{=} \text{ (K)}$ |
|----------------------|--|--|--|--|---------------------|
| ^4He | ^4He van der Waals clusters | 1.46×10^{21} | 0.122 | 3.36 | 0.63 |
| D_2O | type-II clathrate hydrate (90%) | 4.16×10^{21} | 7.43 | 9.57 | 1.09 |
| carbon | hedragonal voids in fcc- C_{60} (70%) | 0.97×10^{21} | 63.9 | 2.23 | — |

Table 2: Rate constants for neutron absorption and for production of UCN with 5 m/s, in three media hosting isolated O_2 molecules at low temperature ($g_{-} = 4/3$). All values are given for bulk matter (for the clathrate and the intercalated fcc- C_{60} with the indicated O_2 filling fractions of cages). At the medium temperature $T_{=}$ the rate constants for up-scattering and absorption are equal.

between O_2 molecules separated by ^4He atoms and using the parameters of the Heisenberg interaction given in [37], the spin interaction energy is found to be less than a mK, ensuring the paramagnetic state of such a system.

Even higher O_2 densities may prevail in clathrate hydrates, a special class of inclusion compounds with water molecules forming an ice-like hydrogen bonded network that contains sub-nm sized cavities stabilized by guests of noble gas atoms or a wide range of molecules [38]. Methods of sample preparation of such systems from water ice can be found in refs. [39, 40]. Oxygen molecules stabilize the type-II clathrate hydrate structure that crystallizes in space group $\text{Fd}\bar{3}\text{m}$. Its face centered cubic unit cell with size $a \approx 1.73$ nm possesses 24 cavities (16 with radius 0.395 nm and 8 with radius 0.473 nm), corresponding to a cavity number density of $4.63 \times 10^{21} \text{ cm}^{-3}$. For a filling fraction of 90%, the cages are occupied only with single O_2 molecules, as was established in a neutron diffraction study [41]. An inelastic neutron scattering study on this system has revealed a dispersion-free magnetic excitation with energy 0.4 meV [42]. i.e. close to the zero-field splitting constant $D = 0.491$ meV measured via ESR for gaseous oxygen [28]. Note that the O_2 density is still a factor five lower than in α -oxygen. Using the same argument as for the O_2 - ^4He van der Waals clusters one can expect the system to stay paramagnetic still down to sub-Kelvin temperatures.

Molecular oxygen can also be intercalated in the fcc lattice of crystallized C_{60} molecules. Up to one O_2 molecule per C_{60} unit can be trapped on the octahedral sites, corresponding to a maximum molecular number density of $1.38 \times 10^{21} \text{ cm}^{-3}$. A neutron scattering study performed on a system prepared with 70% site occupancy has established a dispersion-free magnetic mode with energy 0.4 meV [43], i.e. as observed in the O_2 -hydrate clathrate. This is a strong hint that in both cases the excitation is caused by the zero-field splitting in the oxygen molecule, slightly shifted due to environmental perturbation of the molecular Hamiltonian.

Table 2 quotes, for the media discussed above, the rate constants for neutron conversion to a typical UCN with a speed of 5 m/s and for absorption, according to eqs. 16 and 18. While the van der Waals system has the lowest absorption, the clathrate hydrate converts neutrons fastest. The intercalated C_{60} system has the strongest absorption due to the large abundance of carbon nuclei, and the smallest conversion. On the other hand, still stable at room temperature, it might be the easiest to deal with. Rate constants for neutron up-scattering (see eq. 17) are shown in Fig. 2, from which one can read off values for the temperature $T_{=}$ where the break-even with absorption occurs, i.e. $\tau_{\text{up}}^{-1} = \tau_{\text{a}}^{-1}$. They are also listed in Table 2 (note that for the C_{60} system the absorption is too large for a break-even to exist). Although, due to eq. ??, one can always arrange for $\tau_{\text{up}}^{-1} \ll \tau_{\text{a}}^{-1}$, the intended technical implementation of the moderator will set practical limits. The answer of the question beyond which medium temperature the up-scattering becomes a nuisance depends on the time the converted neutrons have to travel in the material before escape, and hence on the neutron speed and the size of the converter. Obviously, for a small converter the requirements are weaker than for a big moderator discussed further below.

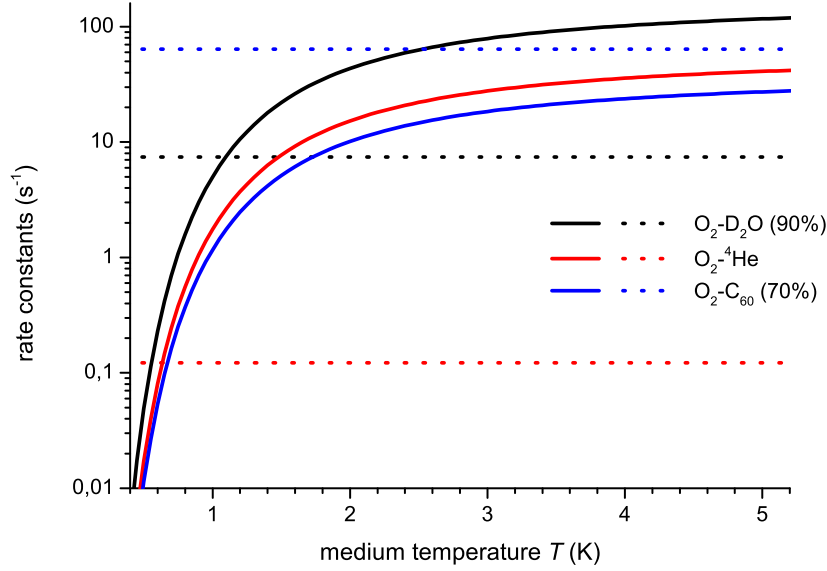


Figure 2: Rate constants τ_{up}^{-1} for neutron up-scattering (solid lines) and τ_{a}^{-1} for neutron absorption (dotted) for the three paramagnetic inclusion compounds of molecular oxygen listed in Table 2.

For a comparison of neutron conversion rates in different materials it is useful to refer to an incident Maxwellian neutron spectrum characterized by a temperature T_{n} and with density given by

$$n(E, T_{\text{n}}) dE = \frac{2}{\sqrt{\pi}} \frac{n}{(k_{\text{B}} T_{\text{n}})^{3/2}} \exp\left(-\frac{E}{k_{\text{B}} T_{\text{n}}}\right) \sqrt{E} dE, \quad (19)$$

where

$$n = \int_0^{\infty} n(E, T_{\text{n}}) dE \quad (20)$$

is the total neutron density [33]. It is related to the total flux by

$$\Phi = \frac{2}{\sqrt{\pi}} n \sqrt{\frac{2k_{\text{B}} T_{\text{n}}}{m_{\text{n}}}}. \quad (21)$$

A well understood medium for neutron conversion is pure superfluid ^4He at saturated vapor pressure. It was first analysed by Pendlebury [44], and we use it as a benchmark here. Neutrons may become converted to UCN if they have an energy of about $E^* \approx 1$ meV (corresponding to wavenumber $k^* \approx 7 \text{ nm}^{-1}$) where the neutron and helium dispersion curves cross each other. Neglecting a small contribution due to multi-phonon processes [45, 46, 47], the UCN conversion rate follows from eq. 3.37 in ref. [7], which after integration over energy can be written as

$$p_{\text{He}} = \frac{2}{3} \Phi n_{\text{He}} \sigma_{\text{He}} S(k^*) \alpha E_{\text{c}}^{3/2} \exp\left(-\frac{E^*}{k_{\text{B}} T_{\text{n}}}\right) \frac{\sqrt{E^*}}{(k_{\text{B}} T_{\text{n}})^2} \quad (22)$$

where $n_{\text{He}} \approx 2.18 \times 10^{22} \text{ cm}^{-3}$ is the ^4He atom density, $\sigma_{\text{He}} \approx 1.34$ barn is the coherent scattering cross section per helium atom, $S(k^*) \approx 0.105$ is the static structure factor of superfluid ^4He at k^* [48], and $\alpha \approx 1.45$ accounts for the overlap of the two dispersion curves. The factor $E_{\text{c}}^{3/2}$ is the same as appearing in the similar expression given in eq. 12. Figure 3 shows that,

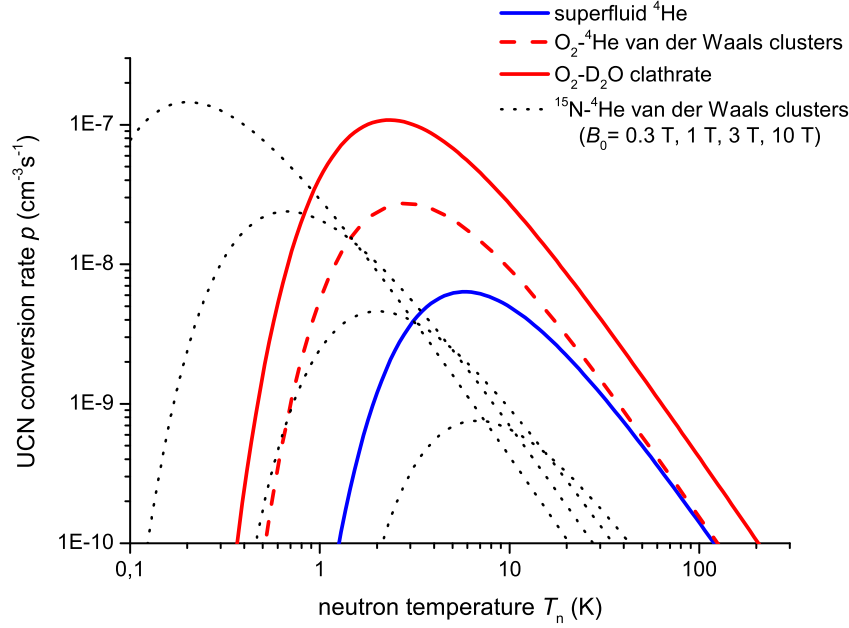


Figure 3: Rates of neutron conversion to UCN with energy up to $E_c = 250$ neV, calculated using eq. 12 in the low-temperature limit with parameters for the various systems as given in Table 2 (we set $E^* = 0.49$ meV for the O_2 - ^4He van der Waals clusters), and eq. 22 for superfluid ^4He . The neutron flux is set to $\Phi = 1 \text{ cm}^{-2}\text{s}^{-1}$. Calculations for the ^{15}N - ^4He van der Waals clusters are done for $1.8 \times 10^{20} \text{ cm}^{-3}$ atomic density of ^{15}N (i.e. the maximum value reported in [35]), for $f_- = 1$, and for values of an external magnetic field B_0 as quoted and corresponding to the dotted curves from left to right.

despite $n_{\text{He}}/n_{\text{pc}} \approx 5$ and for any temperatures of practical interest, the fully deuterated O_2 -hydrate with 90% cage occupancy has a higher UCN conversion rate than superfluid ^4He , which is mainly due to the absence of the unfavorable structure factor $S(k^*)$. For $T_n = 100$ K ($T_n = 30$ K), $p/p_{\text{He}} = 2.9$ (3.4). At neutron temperature close to 6 K, where conversion in superfluid ^4He works best, the clathrate converts neutrons a factor 9 better. The highest conversion in the clathrate appears at an optimum neutron temperature about 2.3 K. Note that the cooling cascade discussed in the next section may enhance production of UCN and VCN in a paramagnetic medium by a further and even larger factor. Note also that the analysis has taken into account only the paramagnetic cross section, neglecting any contribution due to phonons.

3 Paramagnetic cascade cooling of neutrons

For analysis of cascade cooling it is useful to consider first an infinite medium, for which the neutron transport equation takes a particularly simple form. For the sake of a transparent analytical treatment, we consider only the energy transfers in units of E^* due to paramagnetic scattering, neglecting any other inelastic channels and hence underestimating the true moderation efficiency of the material.

We define groups j of neutrons characterized by a spatial density $n_{j,\Delta} dE$ in an energy interval dE about

$$E_j = jE^* + \Delta \quad (23)$$

where $0 \leq \Delta < E^*$ defines a base energy for the lowest group, $j = 0$. For simplicity of notation

we will omit the index Δ in the sequel. Note that, in a j -changing scattering process involving non-dispersive excitations, dE does not change. We denote the rate constant for scattering from group j to j' by $\tau_{j \rightarrow j'}^{-1}$. The rate equation for the population of the group j can then be written as

$$\frac{dn_j}{dt} = s_j + n_{j+1}\tau_{j+1 \rightarrow j}^{-1} + n_{j-1}\tau_{j-1 \rightarrow j}^{-1} - n_j\tau_{j \rightarrow j-1}^{-1} - n_j\tau_{j \rightarrow j+1}^{-1} - n_j\tau_a^{-1}. \quad (24)$$

The term s_j describes homogeneously distributed sources of neutrons. The second and third terms describe feeding due to down-scatters from the group $j+1$ and due to up-scatters from the group $j-1$. The fourth and fifth terms describe losses due to down-scatters to the group $j-1$ and due to up-scatters to the group $j+1$. The last term describes absorption losses with rate constant τ_a^{-1} , which is universal for all groups according to eq. 18 and $\Sigma_a \propto 1/v$. The system of first-order differential equations 24 can be written as

$$\frac{dn_j}{dt} = M_{jk}n_k + s_j, \quad (25)$$

with a tridiagonal matrix

$$\mathbf{M} = \begin{pmatrix} -\tau_{0 \rightarrow 1}^{-1} - \tau_a^{-1} & \tau_{1 \rightarrow 0}^{-1} & 0 & 0 \\ \tau_{0 \rightarrow 1}^{-1} & -\tau_{1 \rightarrow 0}^{-1} - \tau_{1 \rightarrow 2}^{-1} - \tau_a^{-1} & \tau_{2 \rightarrow 1}^{-1} & 0 \\ 0 & \tau_{1 \rightarrow 2}^{-1} & -\tau_{2 \rightarrow 1}^{-1} - \tau_{2 \rightarrow 3}^{-1} - \tau_a^{-1} & \tau_{3 \rightarrow 2}^{-1} \\ 0 & 0 & \tau_{2 \rightarrow 3}^{-1} & -\tau_{3 \rightarrow 2}^{-1} - \tau_{3 \rightarrow 4}^{-1} - \tau_a^{-1} \\ & & \dots & \ddots \end{pmatrix} \quad (26)$$

of constant coefficients (the value of Δ is kept fixed). Stationary solutions are given by

$$n_j = -(\mathbf{M}^{-1})_{jk} s_k. \quad (27)$$

We assume that the sources emit neutrons with a Maxwellian spectrum as given in eq. 19 and define accordingly

$$s_j = \frac{2}{\sqrt{\pi}} \frac{n}{\tau} \frac{\sqrt{E_j}}{(k_B T_n)^{3/2}} \exp\left(-\frac{E_j}{k_B T_n}\right). \quad (28)$$

The source strength is characterized by the density rate $n\tau^{-1}$. The rate constants for neutron up- and down-scattering from the group j follow from

$$\tau_{j \rightarrow j \pm 1}^{-1} = v_j \int_0^\infty \Sigma^\pm(E \rightarrow E_{j \pm 1}) dE, \quad (29)$$

where

$$v_j = \sqrt{\frac{2E_j}{m_n}} \quad (30)$$

is the speed of neutrons in group j , and Σ^\pm is the macroscopic inelastic scattering cross section from eq. 1. One obtains

$$\tau_{j \rightarrow j \pm 1}^{-1} = n_{pc} \sigma_{mg \pm}(T) f_\pm(E_j) v_{j \pm 1}. \quad (31)$$

Solving the system of linear equations 27 requires inversion of the square matrix \mathbf{M} which can be done only for finite matrix order l . For a source spectrum as given in eq. 28 and for neutron group number $j < l$, not too close to l , values for n_j do converge when calculated using matrices with increasing order. In practice one chooses l large enough to cover a major part of the source spectrum. For instance, $l = 100$ is more than sufficient for $T_n \leq 30$ K. Results of calculations performed that way are shown in Fig. 4, for the fully deuterated O₂-clathrate

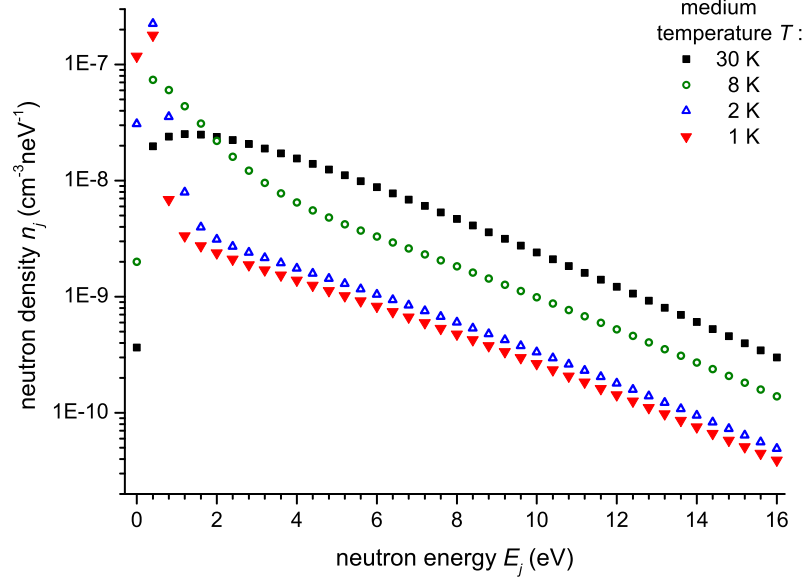


Figure 4: Stationary spectral neutron densities in fully deuterated O₂-clathrate hydrate with 90% cage occupancy, for $T_n = 30$ K and source strength $n\tau^{-1} = 1 \text{ cm}^{-3}\text{s}^{-1}$ (see eq. 28). Each point belongs to a neutron group with energy $jE^* + \Delta$ (shown for $\Delta = 100$ neV).

hydrate held at various temperatures. One can see that, the colder the medium, the more the paramagnetic cooling cascade compresses neutron spectra toward lower neutron energy. One observes also a large enhancement of the group-0 density (here exemplarily shown for UCN with energy 100 neV) by more than two orders of magnitude, with respect to the situation of thermal equilibrium between the moderator and the neutron sources at $T_n = 30$ K. Figure 5 presents stationary neutron densities in the energy region of UCN and VCN, obtained by variation of the offset energy Δ in group 0. Figures 6 and 7 show neutron density spectra calculated for the van der Waals cluster system with an O₂ density as quoted in Table 2 and otherwise the same parameters as used in Figs. 4 and 5. The comparison of the two media complies with the expectation that lower absorption leads to larger neutron densities in the low-energy groups and an increase of the ratio n_0/n_1 due to an improved UCN accumulation in the medium. One can also see that for lower absorption more neutron groups contribute effectively to the cooling as the higher groups get stronger depleted.

It is also interesting to see how the source spectrum temperature T_n influences the shape of the neutron density spectrum in a cold moderator, and in particular its component n_0 . Figure 8 presents examples for the O₂-clathrate hydrate. The values $T_n = 30$ K and 100 K are representative for Maxwellians as frequently employed to approximate the (usually undermoderated) neutron spectra from liquid deuterium or liquid hydrogen cold sources in superpositions with similar weights. The three curves for $T = T_n$ represent spectra of the neutron sources, noting that under this condition the moderator has no influence on the spectral shape. One finds that at $T = T_n = 100$ K (300 K) the density n_0 (again exemplarily taken as UCN with energy 100 neV) is lower than at $T = T_n = 30$ K by a factor of 6 (32), whereas for a cold moderator held at $T = 1$ K, n_0 decreases by only a factor 1.3 (2.8) if $T_n = 100$ K (300 K) instead of 30 K. These numbers tell us that precooling of neutrons by a liquid deuterium or liquid hydrogen cold source is sufficient for the paramagnetic cooling cascade to reach almost its full performance. Direct paramagnetic cooling of thermal neutrons on the other hand involves much longer cas-

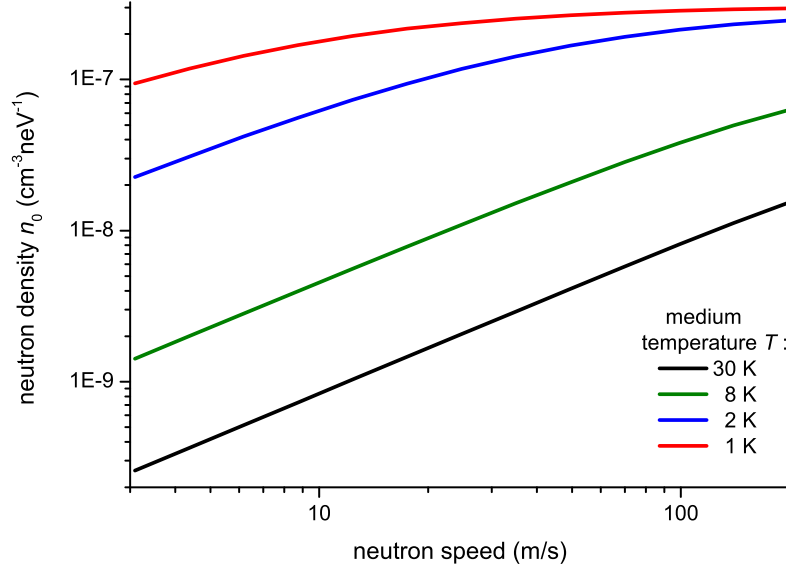


Figure 5: Stationary spectral neutron densities in the lowest neutron group for the fully deuterated O_2 -clathrate hydrate with parameters as in Fig. 4 but energies Δ in the region of UCN and VCN. The range of neutron speed corresponds to $5 \times 10^{-8} \text{ neV} \leq \Delta \leq 2 \times 10^{-4} \text{ neV}$.

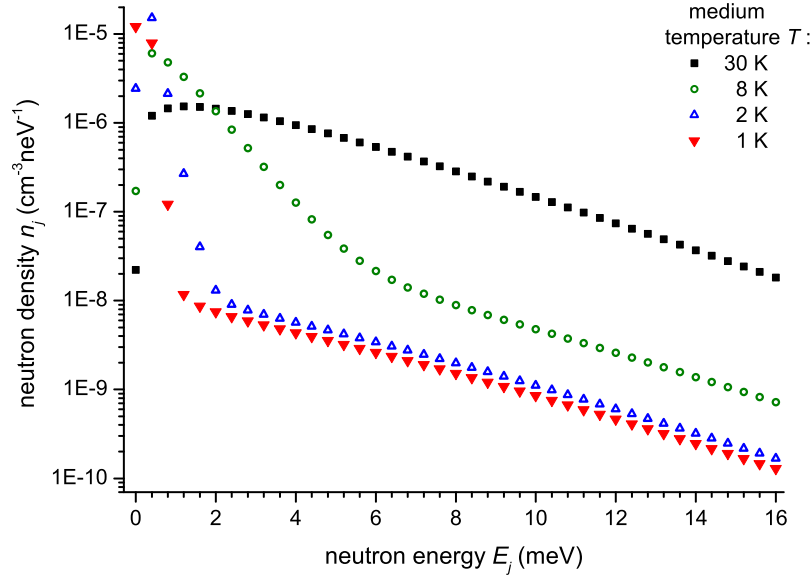


Figure 6: Stationary spectral neutron densities in the O_2 - ^4He van der Waals cluster system with O_2 density $1.46 \times 10^{21} \text{ cm}^{-3}$, for $T_n = 30 \text{ K}$ and source strength $n\tau^{-1} = 1 \text{ cm}^{-3}\text{s}^{-1}$ (see eq. 28). Each point belongs to a neutron group with energy $jE^* + \Delta$ (shown for $\Delta = 100 \text{ neV}$).

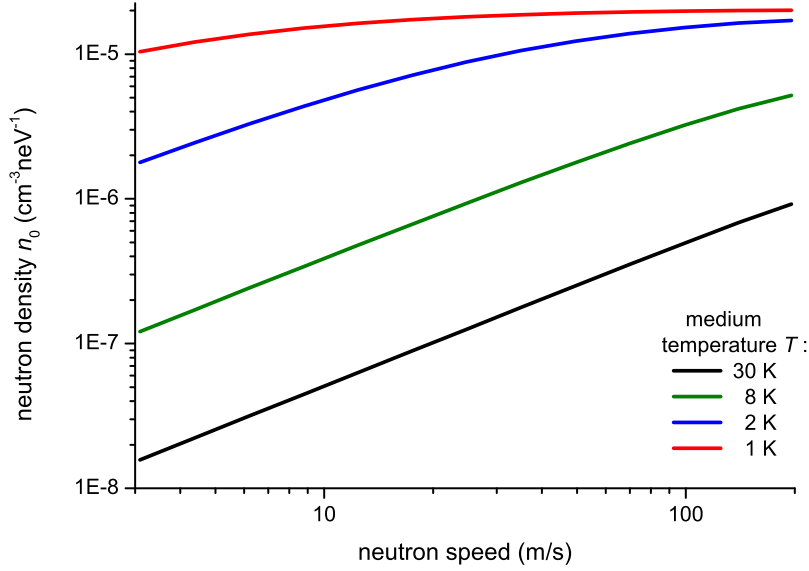


Figure 7: Stationary spectral neutron densities in the lowest neutron group for the $\text{O}_2\text{-}^4\text{He}$ van der Waals system with parameters as in Fig. 6 but energies Δ in the region of UCN and VCN. The range of neutron speed corresponds to $5 \times 10^{-8} \text{ neV} \leq \Delta \leq 2 \times 10^{-4} \text{ neV}$.

acades and suffers from a suppression of the inelastic scattering cross section for large neutron energies due to the magnetic form factor (compare Fig. 1). However, the present analysis still neglects the experimentally studied, non-magnetic excitations in clathrate hydrates [42], which are able to remove many meV of kinetic energy from the neutron in single scattering events. They might shortcut many steps of the paramagnetic cooling process and thereby provide an intrinsic precooling to a degree that a separate cold source could become unnecessary.

From the previous discussion it is qualitatively clear that, the higher T_n , the stronger the relative contribution of the higher-energy neutron groups to the moderated density n_0 . This can indeed be quantified by solving eq. 27 for a system limited to l neutron groups and considering the l dependence of n_0 . The matrix operating on the system of groups, $j = 0$ to $j = l - 1$, has to be properly defined, ensuring the absence of transitions to or from groups with larger j . While simple truncation of \mathbf{M} from eq. 26 to order l removes feeding from groups $j \geq l$, losses to groups $j \geq l$ are avoided by removing the rate constant $\tau_{l \rightarrow l+1}^{-1}$ from the element M_{ll} . We denote the correspondingly modified matrix by $\mathbf{M}_{l \times l}$. For instance,

$$\mathbf{M}_{2 \times 2} = \begin{pmatrix} -\tau_{0 \rightarrow 1}^{-1} - \tau_a^{-1} & \tau_{1 \rightarrow 0}^{-1} \\ \tau_{0 \rightarrow 1}^{-1} & -\tau_{1 \rightarrow 0}^{-1} - \tau_a^{-1} \end{pmatrix} \quad (32)$$

connects only the two lowest neutron groups, $j = 0$ and 1, a situation reminiscent of neutron conversion.

Figure 9 shows densities n_0 as a function of the matrix order l , for the fully deuterated O_2 -clathrate hydrate. One observes only small differences in the l dependence for $T = 0.1 \text{ K}$ and 2 K . Higher temperatures are less interesting if one wants to take advantage of the extraordinary thermal conductance of superfluid helium as a cooling agent for the clathrate (requiring $T < 2.17 \text{ K}$ beyond which the helium becomes a normal liquid at saturated vapor pressure). One can see that for a cold neutron source spectrum at 30 K already eight groups are sufficient to attain half of the saturation density, whereas for $T_n = 100 \text{ K}$ about twenty groups are needed. The

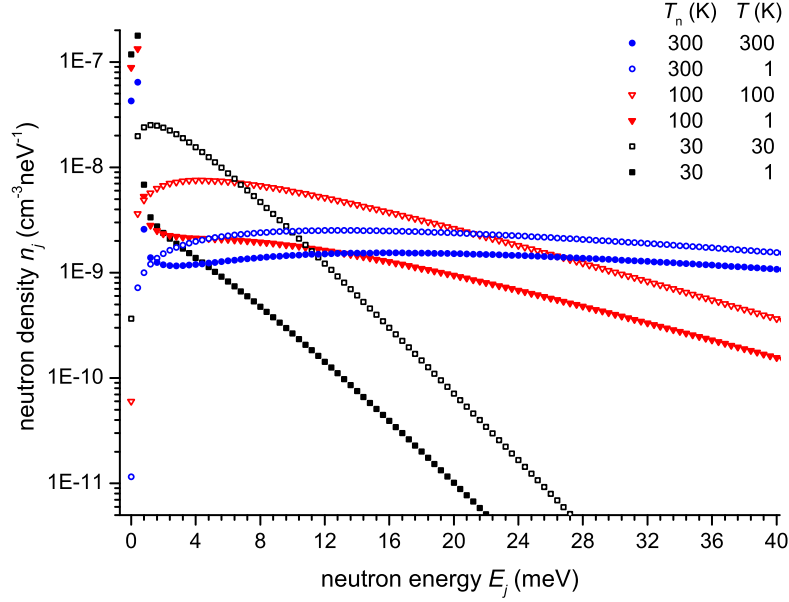


Figure 8: Stationary spectral neutron densities in the fully deuterated O₂-clathrate hydrate with 90% cage occupancy, for various pairs of temperatures (T_n, T) and source strength $n\tau^{-1} = 1 \text{ cm}^{-3}\text{s}^{-1}$ (see eq. 28). Each point belongs to a neutron group with energy $jE^* + \Delta$ (shown for $\Delta = 100 \text{ neV}$).

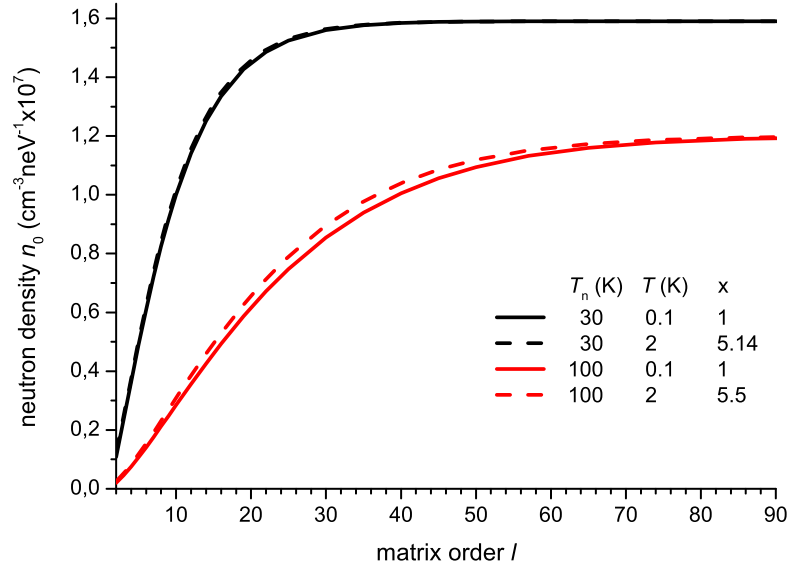


Figure 9: Stationary spectral UCN density (for $\Delta = 100 \text{ neV}$) in the fully deuterated O₂-clathrate hydrate with 90% cage occupancy, as a function of the order l of the matrix $\mathbf{M}_{l \times l}$. The source strength is $n\tau^{-1} = 1 \text{ cm}^{-3}\text{s}^{-1}$ (see eq. 28). Results shown for $T = 2 \text{ K}$ are normalized to the saturation level at $T = 0.1 \text{ K}$ by the respective factor x .

number of groups one wants to participate in the cooling process has impact on the necessary size of a real moderator which is discussed further below.

The effect of the complete cooling cascade can be deduced from comparing the group-0 densities in a large system of groups and in the two-group system with matrix $\mathbf{M}_{2 \times 2}$. We define correspondingly a cascade enhancement factor

$$\eta_{\text{cascade}}(T, T_n) = \frac{n_0(T, T_n, l \rightarrow \infty)}{n_0(T, T_n, l = 2)}. \quad (33)$$

It tells us how much the feeding from the groups $j > 1$ improves the group-0 density. Figure 10 shows cascade enhancements for different temperatures and media. In thermal equilibrium between the moderator and the neutron sources,

$$n_0(T = T_n, l = 2) = n_0(T = T_n, l \rightarrow \infty) \quad (34)$$

as they have to fulfill for a well defined $\mathbf{M}_{l \times l}$. Correspondingly, $\eta_{\text{cascade}}(T = T_n) = 1$. Note that the cascade enhancement accounts only for a part of the effects visible in the figures before. Indeed, the total enhancement of n_0 observed when reducing the temperature T below T_n can be written as

$$\eta = \eta_{\text{cascade}}(T, T_n) \eta_{\text{conv}}(T, T_n), \quad (35)$$

with the factor

$$\eta_{\text{conv}}(T, T_n) = \frac{n_0(T, T_n, l = 2)}{n_0(T = T_n, l = 2)} \quad (36)$$

accounting for the temperature dependence of the medium as a converter. Lowering T leads to $\eta_{\text{conv}}(T, T_n) > 1$ for two reasons. On one hand neutron up-scattering becomes suppressed due to the factor $g_+(T)$ in the cross section. On the other hand, due to its proportionality to $g_-(T)$, the down-scattering cross section increases with the population of the magnetic ground state. For O_2 for instance, $g_-(1 \text{ K}) / g_-(30 \text{ K}) \approx 2.7$.

Finally, we give an estimate for the size a realistic moderator needs to have for the cooling cascade to take effect, noting that the calculations above were performed for an infinite medium. We consider the O_2 -clathrate with 90% cage occupancy held at a temperature low enough that we can neglect up-scattering. While a highly packed state of the clathrate grains can be achieved using a press after clathration, some porosity of the medium will however be useful for cooling the grains with superfluid helium. In the sequel we take a packing fraction $\phi = 0.75$ as a practical value. Relevant quantities for this discussion are the macroscopic cross sections Σ_{ie} , Σ_{e} and Σ_{a} for inelastic and elastic scattering for the neutron groups $j \geq 2$, and for neutron absorption. An estimate for Σ_{ie} follows from eq. 1,

$$\Sigma_{\text{ie}} = n_{\text{pc}} \sigma_{\text{m}} \frac{k'}{k} g_-(T) f_-(E) \approx 0.0076 \text{ cm}^{-1}, \quad (37)$$

where the value on the right side holds for $g_-(T) = 4/3$ and $f_-(E) k'/k = 0.5$. Note that this value underestimates the real cross section for the first seven neutron groups. The elastic cross section Σ_{e} is mainly due to coherent scattering by the packed clathrate crystallites with a contribution due to spin incoherent scattering by the deuterons. Due to the large size of the fcc elementary cell of the O_2 -clathrate hydrate, the Bragg cutoff wavelength is $\lambda_{\text{B}} \approx 2.0 \text{ nm}$. Since neutrons with energy $E^* = 0.4 \text{ meV}$ have a wavelength of 1.41 nm , any neutron, prior to its final conversion into a UCN or VCN or absorption, will diffuse through the medium. The cross section has a complex energy dependence due to the Bragg edges. For an estimate we use (see, e.g., ref. [2]) an average value given by

$$\Sigma_{\text{e}} \approx n(\text{O}) \sigma_{\text{s}}(\text{O}) + n(\text{D}) \sigma_{\text{s}}(\text{D}) = 0.41 \text{ cm}^{-1}, \quad (38)$$

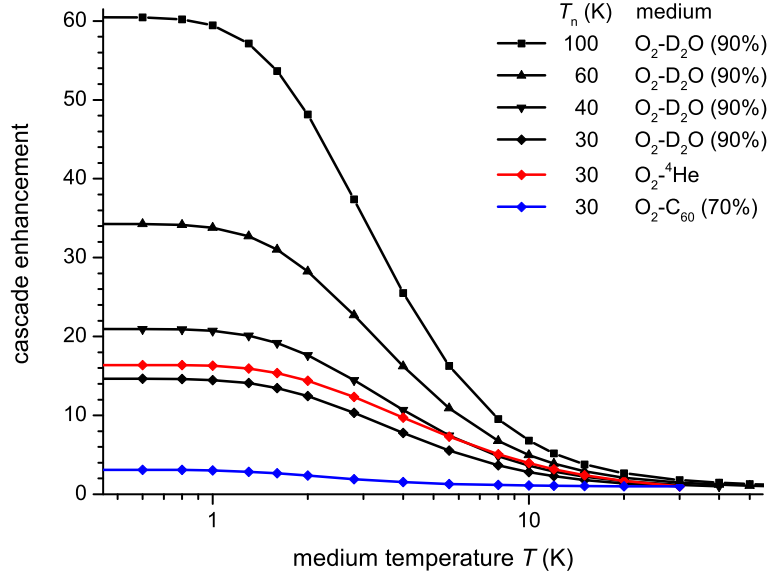


Figure 10: Cascade enhancements as defined in eq. 33, for the paramagnetic media quoted in Table 2.

where $n(\text{O})$ and $n(\text{D})$ are macroscopic averages of atomic number densities of oxygen and deuterium, and $\sigma_s(\text{O}) \approx 4.23$ barn and $\sigma_s(\text{D}) \approx 7.64$ barn are the total scattering cross sections per oxygen and deuterium atom. The macroscopic absorption cross section in neutron group j is given by

$$\Sigma_a = \frac{2200}{277\sqrt{j}} \times [n(\text{O})\sigma_a(\text{O}) + n(\text{D})\sigma_a(\text{D})] \leq 0.00014 \text{ cm}^{-1}, \quad (39)$$

where $\sigma_a(\text{O})$ and $\sigma_a(\text{D})$ are the atomic absorption cross sections of oxygen and deuterium for neutrons with a speed of 2200 m/s (see values in Table 1), and the value on the right is for $j \geq 2$. The cross sections are thus hierarchically ordered as

$$\Sigma_a \ll \Sigma_{ie} \ll \Sigma_e. \quad (40)$$

For multiple inelastic scattering events of the cooling cascade to take place, the moderator needs to be sufficiently large. In analogy to the diffusion length with respect to neutron absorption [33], we define here a quantity

$$L_d = 1/\sqrt{3\Sigma_{ie}(\Sigma_e + \Sigma_{ie})}. \quad (41)$$

It specifies the mean distance \bar{r} between two inelastic scattering events in presence of strong elastic diffusion,

$$\bar{r} = 2L_d. \quad (42)$$

For the cross section estimates quoted above one finds

$$L_d \approx 10 \text{ cm}, \quad (43)$$

so that a fully deuterated O_2 -clathrate hydrate moderator with linear extension D_{mod} less than a meter should provide efficient paramagnetic cascade cooling. Due to up-scattering and absorption (see eqs. 17 and 18), D_{mod} defines a minimum speed that the slowed down, very cold

neutrons need to have for escaping from deep inside the moderator,

$$v_{\text{VCN}} \gtrsim D_{\text{mod}} \tau_{\text{VCN}}^{-1}, \quad (44)$$

with

$$\tau_{\text{VCN}}^{-1} = \tau_{\text{a}}^{-1} + \tau_{\text{up}}^{-1}(T). \quad (45)$$

The rate constants for both loss channels are independent on the neutron speed v_{VCN} (for VCN this statement holds for $E_{\text{VCN}} \ll E^*$) but τ_{up}^{-1} depends on the moderator temperature. A minimum necessary requirement is due to the fact that τ_{up}^{-1} can always be suppressed below τ_{a}^{-1} by choosing T sufficiently low (see Fig. 2 for break-even temperature values for the media discussed before). For an O_2 -clathrate moderator with $D_{\text{mod}} \approx 1$ m one concludes that, even at lowest T , $v_{\text{VCN}} \gtrsim 7.5$ m/s, which is the highest neutron speed in a UCN spectrum defined by a high-potential wall material. Turning around the argument leading to eq. 44, neutrons with lower speed will escape the medium only from within a certain depth from the moderator surface, which may be further reduced if the group-0 neutrons are too strongly diffused [49]. For the moderator held at 0.8 K (1.2 K, 1.5 K, 2 K) the minimum neutron speed as defined by eq. 44 increases to 9 m/s (18.1 m/s, 29.4 m/s, 50.9 m/s). Therefore, we may conclude that the fully deuterated O_2 -clathrate hydrate moderator will be best suited for production of VCN. These may either be used directly, e.g., for an advanced neutron-antineutron search [50] or for various other applications mentioned in the introduction, or be transformed to UCN via gravity and/or a neutron turbine as in ILL's long-standing UCN source.

4 Conclusions

This paper has presented a new mechanism for cooling neutrons well below temperatures attained in liquid hydrogen and deuterium cold sources. Based on the dispersion-free inelastic scattering in a paramagnetic material, neutrons lose kinetic energy in constant steps E^* defined by electronic Zeeman energy or zero-field splittings of molecular magnetic levels. The analytical expressions derived here reveal large possible gains in the production of VCN and UCN with respect to the single-step neutron conversion. A particularly promising medium is the weakly neutron absorbing, fully deuterated type-II clathrate hydrate stabilized by molecular oxygen. Its magnetic excitation at 0.4 meV is well placed to turn neutrons from a cold source into VCN or UCN in a cascade of some dozen collisions. A helpful peculiarity is the large Bragg cutoff wavelength of the clathrate crystallites, $\lambda_{\text{B}} \approx 2.0$ nm; neutrons that still can impart kinetic energy to the moderator, i.e. those with $E > E^*$ and correspondingly $\lambda < 1.4$ nm, will be confined in the moderator by strong diffusion. Also very helpful from a practical point of view is the fact that neutron up-scattering becomes insignificant already at ordinary liquid helium temperatures.

For a neutron spectrum prepared by a common cold source and for an inelastic diffusion length in the order of 10 cm, the paramagnetic cooling cascade will take effect in a moderator with linear dimensions less than a meter. This size should be considered as an upper limit since non-magnetic degrees of freedom were neglected, leading to an underestimate of the true moderation efficiency. Indeed, the O_2 -hydrate possesses many excitations on different energy scales, including rotations and librations of encaged O_2 molecules, and the host lattice modes. The low-energy excitations might offer shortcut channels for a faster, less space demanding moderation of a precooled spectrum, thereby limiting the scope of the paramagnetic cooling cascade to few scattering steps at low energy, where the cross section is only slightly reduced by the magnetic form factor. A candidate is the low-energy band of local, Einstein oscillator type modes observed around 4.8 meV [42]. If on the other hand excitations at higher energies are sufficiently effective as well, external premoderation to subthermal neutron temperatures might be unnecessary.

Otherwise there is also the viable option to couple the O_2 -hydrate to a premoderator made of an advanced cold moderator medium, such as solid methane, methane clathrate or mesitylene, all offering better thermalization at low temperature than liquid hydrogen or deuterium [51].

With its aforementioned size, an O_2 -hydrate moderator would fit in thermal columns of TRIGA [52, 53], PULSTAR [54] or WWR [55] type reactor facilities. Also small accelerator based neutron facilities might offer excellent opportunities for study and exploitation [56, 57]. Preparatory studies on neutron conversion can be performed at a neutron beam similar to the experiments described in refs. [58, 59]. By exposing a larger quantity of the paramagnetic medium to the beam one may also demonstrate the cascade gain factor. Cross section measurements for different cage filling fractions (which can be increased beyond 90% by a larger pressure of O_2 during preparation of the clathrate [41]) can tell us if filling with more than one O_2 molecule is a problem or an opportunity for further increasing the moderation efficiency. A further point to be studied is the transparency of the medium for neutrons having reached wavelengths $\lambda > \lambda_B$ after the final cooling step. This will depend on the level of inhomogeneity scattering [49] due to the mesostructure, determined by size, packing and microporosity of clathrate grains [40]. For implementation of the material in intense neutron fields also the question of radiation damage needs to be addressed.

An "in-pile" O_2 -hydrate moderator may provide highest fluxes of VCN and UCN. Highest ultimate UCN densities might however be attained in pure superfluid ^4He due to its vanishing neutron absorption, enabling UCN accumulation prior to extraction from the converter [60]. Also in this situation the clathrate may become an asset, as a moderating reflector around a superfluid ^4He UCN source placed at the end of a neutron guide [61, 62]. Keeping the clathrate at 6 K, the spectrum of an incident neutron beam will be compressed to provide an optimum density at 1 meV, where the one-phonon process for UCN production in superfluid ^4He takes effect.

Among the other media considered in this paper, also the dry O_2 - ^4He van der Waals cluster system deserves further investigation for its much lower absorption. As this material becomes unstable at much lower temperatures than the O_2 -hydrate (see a phase diagram for the similar N_2 -hydrate in ref. [39]), it might be rather a candidate for implementation at a neutron beam than in-pile. Even more exotic are the paramagnetic atomic Zeeman systems, which however offer a linear dependence of the neutron transfer energy on an applied magnetic field. This degree of freedom might be exploitable in some special experimental situations.

The absence of dispersion in neutron scattering by paramagnetic systems has the additional interesting consequence that neutron conversion to UCN takes place in a narrow energy range of a fraction of a μeV . This strongly contrasts with the dispersive single-phonon emission process in superfluid ^4He , which, for instance for a spectrum up to a cutoff at $E_c = 250$ neV, is kinematically allowed in a wide energy range of 26 μeV about 1 meV [63]. While for the helium case the large mean free path of neutrons with energy 1 meV can in principle be used to enhance the UCN density by a neutron beam resonator [64, 65], the paramagnetic moderator with its narrow energy range for neutron conversion is amenable to beam bunching techniques applicable for pulsed neutron sources, as described in ref. [66]. We finally note that it might also be worthwhile to consider the combination of paramagnetic neutron cooling with Namiot's original proposal, thus putting into practice a two-stage neutron cascade cooler in which the spin dependent nuclear scattering compresses the neutron phase space at lowest energies.

5 Appendix: Neutron scattering cross sections

In this appendix we derive the inelastic neutron scattering cross sections needed for the analysis of neutron conversion and cascade cooling by paramagnetic centers. The first part covers simple Zeeman systems of atomic or ionic paramagnetic centers without zero-field splittings. The

second part deals with the triplet state of molecular oxygen without external magnetic field. The analysis follows standard procedures presented in textbooks on neutron scattering theory [26, 27] up to the point, where we evaluate the thermal averages of time-dependent spin operators without neglecting energy transfers to or from the neutron. While this can in fact be easily accomplished for paramagnetic systems, expressions for such inelastic cross sections seem not to appear in the literature, probably because the usually small energy transfer in the diffuse scattering associated with an electron spin flip is only of limited interest for structural studies. As argued in the main text, the inelastic neutron scattering due to the zero-field splitting in oxygen seems to have already been observed in two experimental studies [42, 43], where it was however tentatively interpreted as a crystal field effect. Also for this reason a comprehensive presentation of the corresponding cross sections seems useful.

5.1 Spin dependent neutron scattering cross sections for a Zeeman system without zero-field splittings

We analyze neutron scattering by atomic or ionic paramagnetic centers polarized in a static external magnetic field and derive partial cross sections for electron spin flip and electron non-spin flip processes, with and without neutron spin flip. We start from the double differential cross section for magnetic neutron scattering in first order time dependent perturbation theory, which is given by

$$\left(\frac{d^2\sigma}{d\Omega dE'} \right)_{\eta \rightarrow \eta'} = \frac{k'}{k} \left(\frac{m_n}{2\pi\hbar^2} \right)^2 \sum_{\lambda\lambda'} p_\lambda |\langle \mathbf{k}'\eta'\lambda' | \mathcal{H}_m(\mathbf{r}) | \mathbf{k}\eta\lambda \rangle|^2 \delta(E_{\lambda'} - E_\lambda + E' - E). \quad (46)$$

Here a neutron with mass m_n , wavevector \mathbf{k} , kinetic energy E and quantum number η for the projection of the neutron spin onto the z axis defined by the external, static magnetic field $\mathbf{B}_0 = (0, 0, B_0)$, is scattered into a final state with \mathbf{k}' , E' and η' . The probed system undergoes a transition from an initial state $|\lambda\rangle$ characterized by a set of quantum numbers λ and energy E_λ to a final state characterized by λ' and energy $E_{\lambda'}$. The cross section in eq. 46 includes a sum over final states λ' and thermal averaging over the initial states by means of statistical weight factors p_λ .

The Hamiltonian $\mathcal{H}_m(\mathbf{r}) = -\boldsymbol{\mu}_n \cdot \mathbf{B}(\mathbf{r})$ of the interaction of the neutron magnetic moment $\boldsymbol{\mu}_n = g_n\mu_N\boldsymbol{\sigma}/2$ with the local magnetic field $\mathbf{B}(\mathbf{r})$ in the paramagnetic system has matrix elements between plane wave states \mathbf{k} and \mathbf{k}' that can be expressed as

$$\mathcal{H}_m(\boldsymbol{\kappa}) = \langle \mathbf{k}' | \mathcal{H}_m(\mathbf{r}) | \mathbf{k} \rangle = \frac{1}{2} \mu_0 g_n \mu_N g_e \mu_B \boldsymbol{\sigma} \cdot \mathbf{Q}_\perp(\boldsymbol{\kappa}), \quad (47)$$

where μ_0 is the magnetic vacuum permeability, $g_n \approx -3.826$ is the g-factor of the neutron, μ_N is the nuclear magneton, $g_e \approx -2.002$ is the g-factor of the electron, μ_B is the Bohr magneton, $\boldsymbol{\sigma}/2$ is the neutron spin in units of \hbar expressed by the vector of Pauli matrices $\boldsymbol{\sigma} = (\sigma_x, \sigma_y, \sigma_z)$, and the scattering vector

$$\boldsymbol{\kappa} = \mathbf{k} - \mathbf{k}' \quad (48)$$

is the momentum transfer to the scattering system in units of \hbar . The vector

$$\mathbf{Q}_\perp = \hat{\boldsymbol{\kappa}} \times (\mathbf{Q} \times \hat{\boldsymbol{\kappa}}) = \mathbf{Q} - (\mathbf{Q} \cdot \hat{\boldsymbol{\kappa}}) \hat{\boldsymbol{\kappa}} \quad (49)$$

is the component of a vector \mathbf{Q} perpendicular to $\boldsymbol{\kappa}$ ($\hat{\boldsymbol{\kappa}}$ is the unit vector of $\boldsymbol{\kappa}$), which can be shown to be in general proportional to the Fourier transform of the atomic magnetization $\mathbf{M}(\mathbf{r})$ due to both, spin and orbital angular momentum of the unpaired electrons. We can limit our attention to the case where unpaired electrons are located close to equilibrium positions of paramagnetic centers, and where individual electron spins of the center j couple to a total spin

\mathbf{S}_j with quantum number S . For the weakly absorbing species quoted in Table 1 the total orbital angular momentum \mathbf{L}_j vanishes. For low-energy neutron scattering S is a conserved quantum number while its z component, characterized by a quantum number m , may change by one unit. Under these circumstances the vector \mathbf{Q} can be shown to take the form

$$\mathbf{Q} = \sum_j \mathbf{Q}_j = \sum_j F_j(\boldsymbol{\kappa}) \exp(i\boldsymbol{\kappa} \cdot \mathbf{R}_j) \mathbf{S}_j, \quad (50)$$

wherein \mathbf{R}_j denotes the position of the j th paramagnetic center and

$$F_j(\boldsymbol{\kappa}) = \int \tilde{s}_j(\mathbf{r}) \exp(i\boldsymbol{\kappa} \cdot \mathbf{r}) d^3r \quad (51)$$

is the magnetic form factor with \tilde{s}_j denoting the density of unpaired electrons of the j th ion, divided by their number, so that $F_j(0) = 1$.

The cross section is given in eq. 46 for specific transitions between neutron spin states $|+\rangle$ and $|-\rangle$ with respect to the external magnetic field. From the standard representation of the Pauli matrices the corresponding matrix elements follow as

$$\langle + | \boldsymbol{\sigma} \cdot \mathbf{Q}_\perp | + \rangle = Q_{\perp z}, \quad \langle - | \boldsymbol{\sigma} \cdot \mathbf{Q}_\perp | - \rangle = -Q_{\perp z}, \quad (52)$$

and

$$\langle - | \boldsymbol{\sigma} \cdot \mathbf{Q}_\perp | + \rangle = Q_{\perp x} + iQ_{\perp y}, \quad \langle + | \boldsymbol{\sigma} \cdot \mathbf{Q}_\perp | - \rangle = Q_{\perp x} - iQ_{\perp y}, \quad (53)$$

with the first (second) pair describing transitions without (with) neutron spin flip. Considering first the cross sections for magnetic neutron spin flip scattering, we use eqs. 47 and 53 in eq. 46 and write

$$\left(\frac{d^2\sigma}{d\Omega dE'} \right)_{\pm \rightarrow \mp} = b_m^2 \frac{k'}{k} \sum_{\lambda\lambda'} p_\lambda \langle \lambda | Q_{\perp x}^\dagger \mp iQ_{\perp y}^\dagger | \lambda' \rangle \langle \lambda' | Q_{\perp x} \pm iQ_{\perp y} | \lambda \rangle \delta(E_{\lambda'} - E_\lambda + E' - E), \quad (54)$$

where

$$b_m = \frac{1}{2} \mu_0 g_n \mu_N g_e \mu_B \frac{m_n}{2\pi\hbar^2} = 5.404 \text{ fm} \quad (55)$$

is the magnetic scattering length. Continuing to follow the standard procedure to evaluate the cross section, the δ function is expressed as

$$\delta(E_{\lambda'} - E_\lambda + E' - E) = \frac{1}{2\pi\hbar} \int_{-\infty}^{\infty} \exp(i(E_{\lambda'} - E_\lambda)t/\hbar) \exp(i(E' - E)t/\hbar) dt. \quad (56)$$

Since $|\lambda\rangle$ are eigenstates of the Hamiltonian \mathcal{H}_0 of the system,

$$\exp(i\mathcal{H}_0 t/\hbar) |\lambda\rangle = \exp(iE_\lambda t/\hbar) |\lambda\rangle. \quad (57)$$

One can define time dependent operators as

$$Q_{\perp\alpha}(t) = \exp(i\mathcal{H}_0 t/\hbar) Q_{\perp\alpha} \exp(-i\mathcal{H}_0 t/\hbar), \quad (58)$$

where $\alpha = x, y, z$ are cartesian coordinates with the z axis pointing along the external magnetic field. Using eq. 50 with this definition, one can write

$$Q_{\perp\alpha}(t) = \sum_j F_j(\boldsymbol{\kappa}) \exp(i\boldsymbol{\kappa} \cdot \mathbf{R}_j(t)) S_{\perp j\alpha}(t), \quad (59)$$

where

$$\mathbf{S}_{\perp j}(t) = \mathbf{S}_j(t) - (\mathbf{S}_j(t) \cdot \hat{\boldsymbol{\kappa}}) \hat{\boldsymbol{\kappa}}, \quad (60)$$

in analogy to eq. 49. Under the usual assumption that the orientations of the electron spins do not affect positions and motion of the nuclei, the thermal averages can be factorized for the nuclear coordinates and electron spins. Using also the closure relation $\sum |\lambda'\rangle \langle \lambda'| = 1$ and denoting the thermal average $\sum p_\lambda \langle \lambda | \dots | \lambda \rangle$ by brackets $\langle \dots \rangle$, the cross section becomes

$$\left(\frac{d^2 \sigma}{d\Omega dE'} \right)_{\pm \rightarrow \mp} = \frac{b_m^2}{2\pi\hbar} \frac{k'}{k} \int_{-\infty}^{\infty} \sum_{jj'} \langle \exp(-i\boldsymbol{\kappa} \cdot \mathbf{R}_{j'}) \exp(i\boldsymbol{\kappa} \cdot \mathbf{R}_j(t)) \rangle F_{j'}^*(\boldsymbol{\kappa}) F_j(\boldsymbol{\kappa}) \\ \times \langle (S_{\perp j'x} \mp iS_{\perp j'y})(S_{\perp jx}(t) \pm iS_{\perp jy}(t)) \rangle \exp(i(E' - E)t/\hbar) dt. \quad (61)$$

It will be useful to employ the raising and lowering operators defined by

$$S_j^\pm = S_{jx} \pm iS_{jy}, \quad (62)$$

which fulfill the relation

$$S_{j'x}S_{jx}(t) + S_{j'y}S_{jy}(t) = \frac{1}{2} \left(S_{j'}^+ S_j^-(t) + S_{j'}^- S_j^+(t) \right). \quad (63)$$

For further evaluation of the spin operator products in the cross section one notes that for a paramagnetic system in an external magnetic field applied in z direction, the total z component of the electron spin is a constant of motion, and therefore

$$\sum_j [S_{jz}, \mathcal{H}_0] = 0. \quad (64)$$

The operators S_j^\pm then change the z component of the total spin of the system by one unit so that

$$\langle S_{j'}^+ S_j^+(t) \rangle = \langle S_{j'}^- S_j^-(t) \rangle = 0, \quad (65)$$

and therefore also

$$\langle S_{j'x}S_{jy}(t) + S_{j'y}S_{jx}(t) \rangle = \frac{1}{2i} \langle S_{j'}^+ S_j^+(t) + S_{j'}^- S_j^-(t) \rangle = 0. \quad (66)$$

Also,

$$\langle S_{j'z}S_{jx}(t) \rangle = 0, \quad \langle S_{j'z}S_{jy}(t) \rangle = 0, \quad (67)$$

and due to equivalence of the x and y axes,

$$\langle S_{j'x}S_{jx}(t) \rangle = \langle S_{j'y}S_{jy}(t) \rangle. \quad (68)$$

Since for a paramagnet there are no correlations between spins of different centers $j \neq j'$,

$$\langle S_{j'\alpha}S_{j\alpha}(t) \rangle = \langle S_{j'\alpha} \rangle \langle S_{j\alpha} \rangle + \delta_{jj'} (\langle S_{j\alpha}S_{j\alpha}(t) \rangle - \langle S_{j'\alpha} \rangle \langle S_{j\alpha} \rangle). \quad (69)$$

In presence of a static magnetic field in z direction, $\langle S_{jz} \rangle \neq 0$ but $\langle S_{jx} \rangle = \langle S_{jy} \rangle = 0$. The spin correlation functions entering the cross section are thus given by

$$\langle S_{j'x}S_{jx}(t) \rangle = \langle S_{j'y}S_{jy}(t) \rangle = \delta_{jj'} \langle S_x S_x(t) \rangle, \quad (70)$$

and

$$\langle S_{j'z}S_{jz}(t) \rangle = \langle S_z \rangle^2 + \delta_{jj'} (\langle S_z S_z(t) \rangle - \langle S_z \rangle^2), \quad (71)$$

where by omission of the index j we focus attention on a medium containing a single paramagnetic species without anisotropy effects due to electrostatic crystal fields. The cross section for neutron spin flip scattering thus becomes

$$\begin{aligned} \left(\frac{d^2\sigma}{d\Omega dE'} \right)_{\eta \neq \eta'} &= \frac{b_m^2}{2\pi\hbar} \frac{k'}{k} \int_{-\infty}^{\infty} \sum_{jj'} \langle \exp(-i\boldsymbol{\kappa} \cdot \mathbf{R}_{j'}) \exp(i\boldsymbol{\kappa} \cdot \mathbf{R}_j(t)) \rangle |F(\boldsymbol{\kappa})|^2 \\ &\times \left[\delta_{jj'} \left(\frac{1}{4} (1 + \hat{\kappa}_z^4) \langle S^+ S^- (t) + S^- S^+ (t) \rangle + (\hat{\kappa}_z^2 - \hat{\kappa}_z^4) (\langle S_z S_z (t) \rangle - \langle S_z \rangle^2) \right) \right. \\ &\left. + (\hat{\kappa}_z^2 - \hat{\kappa}_z^4) \langle S_z \rangle^2 \right] \times \exp(i(E' - E)t/\hbar) dt. \end{aligned} \quad (72)$$

where we have written $\eta \neq \eta'$ instead of $\pm \rightarrow \mp$, since the cross section is found to be independent on the neutron's spin flipping from up to down or vice versa, in contrast to nuclear scattering by polarized nuclei. The cross section for magnetic neutron non spin flip scattering can be derived accordingly, with the replacement of the matrix element product in eq. 54 by $\langle \lambda | Q_{\perp z}^\dagger | \lambda' \rangle \langle \lambda' | Q_{\perp z} | \lambda \rangle$. This results in

$$\begin{aligned} \left(\frac{d^2\sigma}{d\Omega dE'} \right)_{\eta=\eta'} &= \frac{b_m^2}{2\pi\hbar} \frac{k'}{k} \int_{-\infty}^{\infty} \sum_{jj'} \langle \exp(-i\boldsymbol{\kappa} \cdot \mathbf{R}_{j'}) \exp(i\boldsymbol{\kappa} \cdot \mathbf{R}_j(t)) \rangle |F(\boldsymbol{\kappa})|^2 \\ &\times \left[\delta_{jj'} \left(\frac{1}{4} (\hat{\kappa}_z^2 - \hat{\kappa}_z^4) \langle S^+ S^- (t) + S^- S^+ (t) \rangle + (1 - \hat{\kappa}_z^2)^2 (\langle S_z S_z (t) \rangle - \langle S_z \rangle^2) \right) \right. \\ &\left. + (1 - \hat{\kappa}_z^2)^2 \langle S_z \rangle^2 \right] \times \exp(i(E' - E)t/\hbar) dt. \end{aligned} \quad (73)$$

The time dependence of the spin observables is governed by the Hamiltonian of a paramagnetic center in the external magnetic field, i.e.

$$\mathcal{H}_0 = -g\mu_B B_0 S_z. \quad (74)$$

The energy levels are given by the eigenstates of S_z with quantum number m ,

$$\mathcal{H}_0 |m\rangle = E_m |m\rangle, \quad (75)$$

with

$$E_m = -g\mu_B B_0 m. \quad (76)$$

The g-factors of the paramagnetic centers listed in Table 1 are $g \approx -2$. Energy transfers to or from the neutron may occur in units of the Zeeman energy denoted as

$$E^* = |g\mu_B B_0|. \quad (77)$$

The system in thermal equilibrium at temperature T is characterized by a partition function Z , with the population probabilities of the states $|m\rangle$ given by

$$p_m = \frac{\exp(-\beta E_m)}{Z}, \quad Z = \sum_m \exp(-\beta E_m), \quad (78)$$

where the sum extends over the values $-S \leq m \leq S$, and

$$\beta = (k_B T)^{-1} \quad (79)$$

with the Boltzmann constant k_B .

Evaluating first the matrix elements of operators S_z in eqs. 72 and 73, we note that

$$\langle S_z \rangle = \sum_m p_m \langle m | S_z | m \rangle = \sum_m p_m m \quad (80)$$

and

$$\langle S_z S_z(t) \rangle = \sum_m p_m \langle m | S_z S_z(t) | m \rangle = \sum_m p_m m^2 = \langle S_z^2 \rangle \quad (81)$$

are both time independent and thus describe scattering without electronic spin flip. The partition function of the Zeeman system is given by

$$Z = \sum_m \exp(-mx) = \frac{\sinh\left(\left(S + \frac{1}{2}\right)x\right)}{\sinh \frac{x}{2}}, \quad x = -\beta g \mu_B B_0, \quad (82)$$

from which, using eqs. 80 and 81, follow the thermal average values of the spin observables S_z and S_z^2 as

$$\begin{aligned} \langle S_z \rangle &= \frac{1}{Z} \sum_m m \exp(-mx) = -\frac{1}{Z} \frac{dZ}{dx} \\ &= -\frac{1}{2} \left((2S+1) \coth\left(\frac{x}{2}(2S+1)\right) - \coth \frac{x}{2} \right), \end{aligned} \quad (83)$$

and

$$\begin{aligned} \langle S_z^2 \rangle &= \frac{1}{Z} \sum_m m^2 \exp(-mx) = \frac{1}{Z} \frac{d^2 Z}{dx^2} \\ &= S(S+1) + \langle S_z \rangle \coth \frac{x}{2}. \end{aligned} \quad (84)$$

Next we analyze the matrix elements involving the operators S^\pm in eqs. 72 and 73. Application of the time independent operators to a state with quantum number m results in

$$S^\pm |m\rangle = \sqrt{S(S+1) - m(m \pm 1)} |m \pm 1\rangle. \quad (85)$$

Employing the time dependent operators

$$S^\pm(t) = \exp(i\mathcal{H}_0 t/\hbar) S^\pm \exp(-i\mathcal{H}_0 t/\hbar), \quad (86)$$

and using eq. 85 and eq. 86 with eq. 75, we obtain

$$\begin{aligned} \langle S^\pm S^\mp(t) \rangle &= \sum_m p_m \langle m | S^\pm S^\mp(t) | m \rangle \\ &= \sum_m p_m (S(S+1) - m(m \mp 1)) \exp(i(E_{m \mp 1} - E_m)t/\hbar). \end{aligned} \quad (87)$$

These thermal averages thus describe electronic spin flips and associated energy transfer from or to the neutron. Using eqs. 80 and 81 they can be expressed as

$$\langle S^\pm S^\mp(t) \rangle = (S(S+1) - \langle S_z^2 \rangle \pm \langle S_z \rangle) \exp(\pm i g \mu_B B_0 t/\hbar). \quad (88)$$

with the explicit temperature dependences of the thermal averages given in eqs. 83 and 84.

The cross sections given in eqs. 72 and 73 can now be evaluated, using eqs. 63, 81 and 88, with integration over time and collecting the terms that correspond to electronic spin flip and those which do not. We denote the partial cross sections with electronic spin flip leading to a

loss (gain) in neutron energy by a superscript $- (+)$, and those without electronic spin flip by a superscript 0, i.e.

$$\left(\frac{d^2\sigma}{d\Omega dE'}\right)_{\eta \neq \eta'}^{\pm} = \frac{A}{4} (1 + \hat{\kappa}_z^4) (S(S+1) - \langle S_z^2 \rangle \pm \langle S_z \rangle) \delta(E - E' \pm E^*), \quad (89)$$

$$\left(\frac{d^2\sigma}{d\Omega dE'}\right)_{\eta = \eta'}^{\pm} = \frac{A}{4} (\hat{\kappa}_z^2 - \hat{\kappa}_z^4) (S(S+1) - \langle S_z^2 \rangle \pm \langle S_z \rangle) \delta(E - E' \pm E^*), \quad (90)$$

$$\left(\frac{d^2\sigma}{d\Omega dE'}\right)_{\eta \neq \eta'}^0 = A (\hat{\kappa}_z^2 - \hat{\kappa}_z^4) \left(\langle S_z^2 \rangle - \langle S_z \rangle^2 + \langle S_z \rangle^2 \sum_j \exp(i\boldsymbol{\kappa} \cdot \mathbf{R}_j) \right) \delta(E' - E), \quad (91)$$

$$\left(\frac{d^2\sigma}{d\Omega dE'}\right)_{\eta = \eta'}^0 = A (1 - \hat{\kappa}_z^2)^2 \left(\langle S_z^2 \rangle - \langle S_z \rangle^2 + \langle S_z \rangle^2 \sum_j \exp(i\boldsymbol{\kappa} \cdot \mathbf{R}_j) \right) \delta(E' - E). \quad (92)$$

The common factor

$$A = Nb_m^2 \frac{k'}{k} \exp(-2W) |F(\boldsymbol{\kappa})|^2, \quad (93)$$

contains the total number N of paramagnetic centers, and the Debye-Waller factor $\exp(-2W)$, where $2W = \kappa^2 \langle u_{\boldsymbol{\kappa}}^2 \rangle$, and $\langle u_{\boldsymbol{\kappa}}^2 \rangle$ is the mean square displacement of a paramagnetic center in direction of $\boldsymbol{\kappa}$.

The cross sections in eqs. 89 and 90 involving an electron spin flip with energy transfer $\pm E^*$ are incoherent; they do not contain terms due to interferences of amplitudes from different paramagnetic centers. They vanish if the energy of the incident neutron is too small to compensate for the Zeeman energy needed to flip a single electron spin. In the opposite limit, $E \gg E^*$, and if one is not interested in the energy transfer, neglect of E^* in the δ functions and summing up the partial cross sections for electron spin flip and non-spin flip leads to equations found in the text books.

The electron non spin flip cross sections given in eqs. 91 and 92 describe elastic scattering (if neglecting the neutron Zeeman energy in case of neutron spin flip scattering, the approximation adopted here). They contain an incoherent diffuse term and a coherent term proportional to $\langle S_z \rangle^2$ due to interferences of amplitudes from different paramagnetic centers, which may show up in Bragg peaks, or lead to small angle scattering contrast for instance for agglomerations of paramagnetic centers immersed in a non-magnetic solvent. Another noteworthy feature is the fact that the coherent cross section with neutron spin flip does not vanish in directions for which $\hat{\kappa}_z^2 - \hat{\kappa}_z^4 \neq 0$, i.e. when $\boldsymbol{\kappa}$ does not point parallel or perpendicular to the applied magnetic field.

For our calculations on neutron conversion and cooling we are primarily interested in the neutron energy changing total cross sections. After integration of $\hat{\kappa}_z^2$ and $\hat{\kappa}_z^4$ over solid angle,

$$\int \hat{\kappa}_z^2 d\Omega = \frac{4}{3}\pi, \quad \int \hat{\kappa}_z^4 d\Omega = \frac{4}{5}\pi, \quad (94)$$

we can write them as

$$\left(\frac{d\sigma}{dE'}\right)^{\pm} = \left(\frac{d\sigma}{dE'}\right)_{\eta \neq \eta'}^{\pm} + \left(\frac{d\sigma}{dE'}\right)_{\eta = \eta'}^{\pm} = N\sigma_m \frac{k'}{k} \exp(-2W) g_{\pm}(T) f_{\pm}(E) \delta(E \pm E^* - E'), \quad (95)$$

where we have defined $\sigma_m = 4\pi b_m^2 \approx 3.66$ barn and

$$g_{\pm}(T) = \frac{1}{3} (S(S+1) - \langle S_z^2 \rangle \pm \langle S_z \rangle), \quad (96)$$

with $\langle S_z \rangle$ and $\langle S_z^2 \rangle$ given by eqs. 83 and 84. The functions $f_{\pm}(E)$ account for the magnetic form factor, which is discussed in the main text.

5.2 Cross sections for the molecular oxygen spin triplet system

Here we consider magnetic neutron scattering by an assembly of unoriented oxygen molecules with motions frozen out. The molecules are assumed to be kept sufficiently far apart from each other to avoid magnetic ordering. This can be achieved using the cage structures discussed in the main text. Our primary interest is the scattering involving transitions between magnetic levels within the triplet state, which is inelastic due to the molecular zero-field splitting. For unoriented molecules and without external magnetic field there is no global quantization axis in the system. It is therefore appropriate to start from the magnetic scattering cross section for unpolarized neutrons (see, e.g. [27]),

$$\frac{d^2\sigma}{d\Omega dE'} = b_m^2 \frac{k'}{k} \sum_{\alpha\beta} (\delta_{\alpha\beta} - \hat{\kappa}_\alpha \hat{\kappa}_\beta) \sum_{\lambda\lambda'} p_\lambda \langle \lambda | Q_\alpha^\dagger | \lambda' \rangle \langle \lambda' | Q_\beta | \lambda \rangle \delta(E_{\lambda'} - E_\lambda + E' - E), \quad (97)$$

using the same notation of states and transition operators as in the previous section. Each oxygen molecule is characterized by a coordinate \mathbf{R}_j of its center of gravity and relative positions \mathbf{l}_{j1} and \mathbf{l}_{j2} of the two atoms. Projection of the total spin onto the molecular axis, $\mathbf{l}_{j1} - \mathbf{l}_{j2}$, provides a good quantum number. As we do not deal with nuclear scattering, the atomic coordinates do not explicitly occur as variables in the cross section but manifest implicitly as a site dependence of the spin eigenstates. Also the magnetic form factor depends on the molecular orientation, which we can however take as isotropic for our purposes (see section 2). Taking electronic spins and spatial coordinates as independent quantities we write

$$\begin{aligned} \frac{d^2\sigma}{d\Omega dE'} &= \frac{b_m^2}{2\pi\hbar} \frac{k'}{k} |F(\kappa)|^2 \sum_{\alpha\beta} (\delta_{\alpha\beta} - \hat{\kappa}_\alpha \hat{\kappa}_\beta) \times \\ &\times \int_{-\infty}^{\infty} \sum_{jj'} \langle \exp(-i\boldsymbol{\kappa} \cdot \mathbf{R}_{j'}) \exp(i\boldsymbol{\kappa} \cdot \mathbf{R}_j(t)) \rangle \langle S_{j'\alpha} S_{j\beta}(t) \rangle \exp(i(E' - E)t/\hbar) dt. \end{aligned} \quad (98)$$

For uncorrelated oxygen molecules,

$$\langle S_{j'\alpha} S_{j\beta}(t) \rangle = \langle S_{j'\alpha} \rangle \langle S_{j\beta}(t) \rangle = 0 \quad (j \neq j'). \quad (99)$$

We are thus left with a single sum over an assembly of unoriented and independent triplet spin systems,

$$\begin{aligned} \frac{d^2\sigma}{d\Omega dE'} &= \frac{b_m^2}{2\pi\hbar} \frac{k'}{k} \exp(-2W) |F(\kappa)|^2 \times \\ &\times \int_{-\infty}^{\infty} \sum_j \sum_{\alpha\beta} (\delta_{\alpha\beta} - \hat{\kappa}_\alpha \hat{\kappa}_\beta) \langle S_{j\alpha} S_{j\beta}(t) \rangle \exp(i(E' - E)t/\hbar) dt. \end{aligned} \quad (100)$$

The product $\langle \exp(-i\boldsymbol{\kappa} \cdot \mathbf{R}_j) \exp(i\boldsymbol{\kappa} \cdot \mathbf{R}_j(t)) \rangle$ is the Debye-Waller factor denoted by $\exp(-2W)$. In the sum over j any molecular orientation appears with equal weight with respect to the given direction $\hat{\kappa}$, of which the differential cross section is obviously independent. We may therefore define for each molecule its own coordinate system and replace

$$\sum_j \sum_{\alpha\beta} (\delta_{\alpha\beta} - \hat{\kappa}_\alpha \hat{\kappa}_\beta) \langle S_{j\alpha} S_{j\beta}(t) \rangle = N \left\langle \sum_{\alpha\beta} (\delta_{\alpha\beta} - \hat{\kappa}_\alpha \hat{\kappa}_\beta) S_\alpha S_\beta(t) \right\rangle. \quad (101)$$

On the right side the brackets include angular averaging in addition to the thermal averaging over molecular spin states. Accordingly we have omitted the site index j to the spin operators.

For further evaluation we choose local cartesian coordinates with z axis parallel to the molecular axis and take the x and y axes in directions for which their projections on κ are equal, i.e.

$$\hat{\kappa}_x = \hat{\kappa}_y = \frac{1}{\sqrt{2}} \sin \vartheta, \quad \hat{\kappa}_z = \cos \vartheta, \quad (102)$$

where ϑ is the angle between κ and the molecular axis. The triplet states of the oxygen molecule are labelled by quantum numbers $m = -1, 0, +1$ characterizing the spin state projection along the symmetry axis of the molecule. The Hamiltonian (without external magnetic field) is given by

$$\mathcal{H}_0 = DS_z^2 - \frac{2}{3}D, \quad (103)$$

which accounts for the energy difference by the zero-field splitting constant D of the states with $m = \pm 1$ and the $m = 0$ state [67]. It commutes with S_z , and since the spin operators obey the same algebra as in the Zeeman case (with different meaning of the states), with the definition of raising and lowering operators in eq. 62, we use eqs. 63, 66, 67 and 81, and obtain

$$\left\langle \sum_{\alpha\beta} (\delta_{\alpha\beta} - \hat{\kappa}_\alpha \hat{\kappa}_\beta) S_\alpha S_\beta(t) \right\rangle = \frac{1}{3} \langle (S^+ S^- (t) + S^- S^+ (t)) \rangle + \frac{2}{3} \langle S_z^2 \rangle. \quad (104)$$

The eigenenergies of \mathcal{H}_0 are given by

$$E_m = \left(m^2 - \frac{2}{3} \right) D. \quad (105)$$

The partition function as defined in eq. 78 follows as

$$Z = \exp(2x) + 2 \exp(-x), \quad x = \frac{\beta D}{3}. \quad (106)$$

Using eq. 87 with eq. 105, we obtain

$$\langle S^+ S^- (t) + S^- S^+ (t) \rangle = 4 \frac{\exp(iDt/\hbar) + \exp(-\beta D) \exp(-iDt/\hbar)}{1 + 2 \exp(-\beta D)}. \quad (107)$$

The total scattering cross sections with neutron energy loss ($-$), energy gain ($+$) thus become

$$\left(\frac{d\sigma}{dE'} \right)^\pm = N \sigma_m \frac{k'}{k} \exp(-2W) g_\pm(T) f_\pm(E) \delta(E \pm D - E'), \quad (108)$$

where

$$g_-(T) = \frac{4}{3} \frac{1}{1 + 2 \exp(-\beta D)}, \quad (109)$$

and

$$g_+(T) = \frac{4}{3} \frac{\exp(-\beta D)}{1 + 2 \exp(-\beta D)}. \quad (110)$$

The functions $f_\pm(E)$ account for the magnetic form factor as discussed in the main text. The cross sections fulfill the relation of detailed balance, as they have to.

Using eq. 81 we also obtain

$$\langle S_z^2 \rangle = \frac{2}{2 + \exp(\beta D)}, \quad (111)$$

from which follows the (for our present purposes less interesting) elastic cross section as

$$\left(\frac{d\sigma}{dE'} \right)^0 = N \sigma_m \exp(-2W) g_0(T) f_0(E) \delta(E - E'), \quad (112)$$

where

$$g_0(T) = \frac{4}{3} \frac{1}{2 + \exp(\beta D)} \rightarrow 0 \quad (T \rightarrow 0), \quad (113)$$

and

$$f_0(E) = \frac{1}{2} \int_0^\pi \langle |F|^2 \rangle (\kappa_0(E, \theta)) \sin \theta d\theta. \quad (114)$$

The brackets stand for orientational averaging of the molecules, and

$$\kappa_0 = \frac{2}{\hbar} \sqrt{m_n E (1 - \cos \theta)}. \quad (115)$$

References

- [1] P. Ageron, Nucl. Instr. Meth A **284**, 197 (1989).
- [2] I.I. Gurevich and L.V. Tarasov, *Low-energy neutron physics*, North-Holland, Amsterdam (1968).
- [3] V.A. Namiot, Sov. Phys. Dokl. **18**, 481 (1974).
- [4] F.M. Piegsa, Physical Review C **88**, 045502 (2013).
- [5] K. Babu et al., arXiv:1310.8593 (2013).
- [6] F.M. Piegsa, G. Pignol, Phys. Rev. Lett. **108**, 181801 (2012).
- [7] R. Golub, D.J. Richardson, S.K. Lamoreaux, *Ultra-Cold Neutrons*, Adam Hilger (1991).
- [8] V.K. Ignatovich, *The Physics of Ultracold Neutrons*, Oxford Science Publications, Clarendon Press (1990).
- [9] D. Dubbers and M.G. Schmidt, Rev. Mod. Phys. **83**, 1111 (2011).
- [10] M.J. Ramsey-Musolf and S. Su, Phys. Rept. **456**, 1 (2008).
- [11] H. Abele, Prog. Nucl. Phys. **60**, 1 (2008).
- [12] A. Steyerl, H. Nagel, F.-X. Schreiber et al., Phys. Lett. A **116**, 347 (1986).
- [13] T. Lauer, T. Zechlau, Eur. Phys. J. A **49**, 104 (2013).
- [14] A. Frei, Yu. Sobolev, I. Altarev, K. Eberhard et al., Eur. Phys. J. A **34**, 119 (2007).
- [15] A. Saunders, M. Makela, Y. Bagdasaova et al., Rev. Sci. Instrum. **84**, 013304 (2013).
- [16] Y. Masuda, K. Hatanaka, S.-C. Jeong et al., Phys. Rev. Lett. **108**, 134801 (2012).
- [17] B. Lauss, Hyperfine Interactions **211**, 21 (2012).
- [18] O. Zimmer, F.M. Piegsa, S.N. Ivanov, Phys. Rev. Lett. **107**, 134801 (2011).
- [19] O. Zimmer, P. Schmidt-Wellenburg, M. Fertl et al., Eur. Phys. J. C **67**, 589 (2010).
- [20] R. Golub and J.M. Pendlebury, Phys. Lett. **53A**, 133 (1975).
- [21] R. Golub, J. Pendlebury, Phys. Lett. A **82**, 337 (1977).
- [22] R. Golub and K. Böning, Z. Phys. B **51**, 95 (1983).

- [23] E. Gutmiedl, F. Böhle, A. Frei et al., *Europ. Phys. Lett.* **96**, 62001 (2011).
- [24] C.-Y. Liu, A.R. Young, arXiv:nucl-th/0406004 (2004).
- [25] D.J. Salvat, E. Gutmiedl, C.-Y. Liu et al., *Europ. Phys. Lett.* **103**, 12001 (2013).
- [26] S.W. Lovesey, *Theory of neutron scattering from condensed matter*, Clarendon Press, Oxford (1984).
- [27] G.L. Squires, *Introduction to the theory of neutron scattering*, Cambridge University Press (1978).
- [28] M. Tinkham, M.W.P. Strandberg, *Phys. Rev.* **97**, 937 (1955).
- [29] A. Meckler, *J. Chem. Phys.* **21**, 1750 (1953).
- [30] W.H. Kleiner, *Phys. Rev.* **97**, 411 (1955).
- [31] M. Deraman, J.C. Dore, J. Schweizer, *J. Magn. Magn. Mat.* **50**, 178 (1985).
- [32] R.J. Meier, R.B. Helmholtz, *Phys. Rev. B* **29**, 1387 (1984).
- [33] K.H. Beckurts and K. Wirtz, *Neutron physics*, Springer (1964).
- [34] V.B. Efimov, A.N. Izotov, L.P. Mezhev-Deglin, *Bull. Russ. Acad. Sci. Phys.* **77**, 48 (2013).
- [35] E.B. Gordon, V.V. Khmelenko, A.A. Pelemenev, E.A. Popov, O.F. Pugachev, *Chem. Phys.* **155**, 301 (1988).
- [36] E.B. Gordon, V.V. Khmelenko, A.A. Pelemenev, et al., *Chem. Phys.* **170**, 411 (1993).
- [37] Yu.A. Freiman, H.J. Jodl, *Phys. Rep.* **401**, 1 (2004).
- [38] E.D. Sloan, C.A. Koh, *Clathrate hydrates of natural gases*, CRC Press (2008).
- [39] W. F. Kuhs, B. Chazallon, P. G. Radaelli, F. Pauer, *J. Incl. Phenom.* **29**, 65 (1997).
- [40] W. F. Kuhs, A. Klapproth, F. Gotthardt, K. Techmer, T. Heinrichs, *Geophys. Res. Lett.* **27**, 2929 (2000).
- [41] B. Chazallon, W.F. Kuhs, *J. Chem. Phys.* **117**, 308 (2002).
- [42] B. Chazallon, H. Itoh, M. Koza, W.F. Kuhs, H. Schober, *Phys. Chem. Chem. Phys.* **4**, 4809 (2002).
- [43] B. Renker, G. Roth, H. Schober, P. Nagel, R. Lortz, C. Meingast, D. Ernst, M.T. Fernandez-Diaz, M. Koza, *Phys. Rev. B* **64**, 205417 (2001).
- [44] J.M. Pendlebury, private communication (1982).
- [45] P. Schmidt-Wellenburg, K.H. Andersen, O. Zimmer, *Nucl. Instr. Meth. A* **611**, 259 (2009).
- [46] C.A. Baker, S.N. Balashov, J. Butterworth et al., *Phys. Lett. A* **308**, 67 (2003).
- [47] E. Korobkina, R. Golub, B.W. Wehring, A.R. Young, *Phys. Lett. A* **301**, 462 (2002).
- [48] R.A. Cowley, D.B. Woods, *Can. J. Phys.* **49**, 177 (1971).
- [49] A. Steyerl, W.-D. Trüstedt, *Z. Phys.* **267**, 379 (1974).

- [50] A. Young, private communication.
- [51] H. Conrad, W.F. Kuhs, K. Nünninghoff et al., *Physica B* **350**, e647 (2004).
- [52] D.M. Fouquet, J. Razvi, W.L. Whittemore, *Nuclear News* **12**, 46 (2003).
- [53] R. Golub, *Nucl. Instr. Meth. in Phys. Res.* **226**, 558 (1984).
- [54] E.I. Korobkina, B.W. Wehring, A.I. Hawari, A.R. Young et al., *Nucl. Instr. Meth. A* **579**, 530 (2007).
- [55] A.P. Serebrov, V.A. Mityuklaev, A.A. Zakharov et al., *Nucl. Instr. Meth. A* **611**, 276 (2009).
- [56] C.M. Lavelle, D.V. Baxter, A. Bogdanov et al., *Nucl. Instr. Meth. A* **587**, 324 (2008).
- [57] Y. Masuda, T. Kitagaki, K. Hatanaka et al., *Phys. Rev. Lett.* **89**, 284801 (2002).
- [58] F. Atchison, B. van den Brandt, T. Bryś et al., *Phys. Rev. C* **71**, 054601 (2005).
- [59] P. Ageron, W. Mampe, R. Golub, J.M. Pendlebury, *Phys. Lett.* **66A**, 469 (1978).
- [60] O. Zimmer, K. Baumann, M. Fertl et al., *Phys. Rev. Lett.* **99**, 104801 (2007).
- [61] S. Baessler, A.M. Gagarski, E.V. Lychagin et al., *C. R. Physique* **12**, 729 (2011).
- [62] P.D. Bangert, M.D. Cooper, S.K. Lamoreaux, *Nucl. Instr. Meth. A* **410**, 264 (1998).
- [63] H. Yoshiki, *Comp. Phys. Comm.* **151**, 141 (2003).
- [64] O. Zimmer, *Phys. Procedia* **51**, 85 (2014).
- [65] E. Jericha, D.E. Schwab, C.J. Carlile, M.R. Jäkel, R. Loidl, H. Rauch, *Nucl. Instr. Meth. A* **440**, 597 (2000).
- [66] H. Rauch, *Nucl. Instr. Meth. A* **338**, 9 (1994).
- [67] E. Wasserman, L.C. Snyder, W.A. Yager, *J. Chem. Phys.* **41**, 1763 (1964).